Molecular Therapy
Nucleic Acids
Original Article

miR-150-PTPMT1-cardiolipin signaling in pulmonary arterial hypertension

Giusy Russomanno,[1,2] Kyeong Beom Jo,[1] Vahitha B. Abdul-Salam,[1,3] Claire Morgan,[1] Jens Endruschat,[4] Ute Schaeper,[4] Ahmed H. Osman,[1] Mai M. Alzaydi,[1,5] Martin R. Wilkins,[1] and Beata Wojciak-Stothard[1]

[1]National Heart and Lung Institute, Imperial College London, London, UK; [2]Department of Pharmacology and Therapeutics, Institute of Systems, Molecular and Integrative Biology (ISMIB), University of Liverpool, Liverpool, UK; [3]William Harvey Research Institute, Barts and The London School of Medicine and Dentistry, Queen Mary University of London, London, UK; [4]Silence Therapeutics GmbH, Berlin, Germany; [5]National Center for Biotechnology, King Abdulaziz City for Science and Technology (KACST), Riyadh, Saudi Arabia

Circulating levels of endothelial miR-150 are reduced in pulmonary arterial hypertension (PAH) and act as an independent predictor of patient survival, but links between endothelial miR-150 and vascular dysfunction are not well understood. We studied the effects of endothelial miR-150 supplementation and inhibition in PAH mice and cells from patients with idiopathic PAH. The role of selected mediators of miR-150 identified by RNA sequencing was evaluated *in vitro* and *in vivo*. Endothelium-targeted miR-150 delivery prevented the disease in Sugen/hypoxia mice, while endothelial knockdown of miR-150 had adverse effects. miR-150 target genes revealed significant associations with PAH pathways, including proliferation, inflammation, and phospholipid signaling, with PTEN-like mitochondrial phosphatase (PTPMT1) most markedly altered. PTPMT1 reduced inflammation and apoptosis and improved mitochondrial function in human pulmonary endothelial cells and blood-derived endothelial colony-forming cells from idiopathic PAH. Beneficial effects of miR-150 *in vitro* and *in vivo* were linked with PTPMT1-dependent biosynthesis of mitochondrial phospholipid cardiolipin and reduced expression of pro-apoptotic, pro-inflammatory, and pro-fibrotic genes, including *c-MYB*, *NOTCH3*, transforming growth factor β (*TGF-β*), and *Col1a1*. In conclusion, we are the first to show that miR-150 supplementation attenuates pulmonary endothelial damage induced by vascular stresses and may be considered as a potential therapeutic strategy in PAH.

INTRODUCTION

Pulmonary arterial hypertension (PAH) is a severe and currently incurable disease characterized by progressive thickening of small arteries in the lung, leading to increased pulmonary vascular resistance and right heart failure.[1] Endothelial damage followed by proliferation of vascular smooth muscle cells underlie the disease pathology.[2] The converging effects of hypoxia, inflammation, and oxidative and metabolic stress play a key contributory role.

At the cellular level, the arterial and right ventricular (RV) remodeling in PAH is associated with a shift from oxidative phosphorylation to glycolysis,[3] which increases the availability of non-oxidized lipids, amino acids, and sugars essential for rapid cell proliferation.[4] These changes are accompanied by inhibition of mitochondrial biogenesis, mitochondrial fragmentation, membrane hyperpolarization, and altered reactive oxygen species (ROS) production.[4,5]

MicroRNAs (miRNAs) have emerged as essential regulators of multiple cellular processes, simultaneously controlling mRNA processing, stability, and translation of multiple gene targets. Given the multifaceted nature of PAH pathology, there is interest in the role of miRNAs in the pathogenesis of this condition.[6]

We have previously shown that reduced miR-150-5p (referred to as miR-150) levels in plasma, circulating microvesicles, and the blood cell fraction from PAH patients are significant predictors of survival, independent of age, cardiac index, disease duration, and circulating lymphocyte count.[7] While miR-150 is highly expressed in mature lymphocytes, circulating lymphocytes account for only about 6% of the variation in the miR-150 level, suggesting that endothelial cells are a likely source of this miRNA.[8] The impact of variation in endothelial miR-150 expression on endothelial function or disease pathology has not yet been investigated.

Herein, we describe the effects of endothelial miR-150 supplementation and inhibition in experimental PAH, human pulmonary artery endothelial and smooth muscle cells, and blood-derived endothelial colony-forming cells (ECFCs) from PAH patients and identify the signaling mediators involved. We show that miR-150 has anti-apoptotic, anti-inflammatory, anti-proliferative, and anti-fibrotic effects and is required for mitochondrial adaptation to an increased energy demand in conditions of vascular stress.

Received 26 April 2020; accepted 28 October 2020;
https://doi.org/10.1016/j.omtn.2020.10.042.

Correspondence: Beata Wojciak-Stothard, National Heart and Lung Institute, Imperial College London, ICTEM Building, Hammersmith Campus, Du Cane Road, London W12 0NN, UK.
E-mail: wojciak-stothard@imperial.ac.uk

RESULTS

Endothelial supplementation of miR-150 improves pulmonary vascular hemodynamics and reduces vascular remodeling in Sugen/hypoxia mice

As a proof of concept, the potential therapeutic effects of miR-150 administration were evaluated in Sugen/hypoxia PAH mice (Figure 1A). miR-150 complexed with the lipid carrier DACC was delivered via tail vein injection at 4-day intervals throughout the 3-week period of study. The DACC liposomal formulation targets the vascular endothelium, with highest efficiency seen in the lung.[9,10] Analysis of the distribution of fluorescently labeled RNA mimic duplex 1-Cy3 delivered in DACC liposomes 24 h post-injection confirmed that liposomal cargo accumulated in the lung, but also in other tissues, including heart and liver (Figure S1).

The control Sugen/hypoxia animals showed a significantly elevated right ventricular systolic pressure (RVSP), right ventricular hypertrophy (RVH), and increased vascular muscularization, marked by a prominent staining of α-smooth muscle actin (α-SMA) of pre-capillary arterioles (Figures 1B–1E). Lung and heart levels of miR-150 were significantly reduced in these mice when compared with healthy transfection controls (Figures 1F and 1G). Reduction in miR-150 expression was most prominent in the vascular endothelium while miR-150 expression levels in leukocytes and airway epithelium remained relatively unaffected (Figure S2).

Effective miR-150 delivery to lung and heart tissues was confirmed by qPCR (Figures 1F and 1G). The treatment reduced RVSP ($p < 0.05$), RVH ($p < 0.05$), and vascular muscularization ($p < 0.0001$; Figures 1B–1E). To evaluate potential liver toxicity of DACC/miR-150 delivery, aspartate aminotransferase (AST) assay was performed on liver tissues from different study groups (Figure S3). DACC-treated mice showed an ∼2-fold increase in AST activity, comparable to the levels seen in hyperglycemic mice.[11] This mild hepatotoxic effect is more likely to be associated with liposomal liver clearance[12] rather than miR-150, as no significant difference in AST activity was noted between DACC controls and DACC/miR-150-treated mice.

Heterozygous endothelial-specific deletion of miR-150 worsens the symptoms of pulmonary hypertension (PH)

Heterozygous miR-150iEC-knockout (KO) mice (miR-150^{fl}/Cdh5(PAC)-iCreERT2) were used for experiments to mimic the reduction (but not complete depletion) of miR-150 content seen in human disease and pre-clinical models of PAH. Following tamoxifen administration, the efficiency of Cre-recombinase-mediated deletion of miR-150 was confirmed by qPCR (Figure 2A).

Sugen/hypoxia miR-150iEC-KO mice showed a substantial elevation of RVSP (∼2-fold increase, $p < 0.0001$), accompanied by a rise in RVH and pulmonary vascular muscularization (both $p < 0.05$), compared with Sugen/hypoxia wild-type littermates (Figures 2B–2E).

Identification of miR-150-regulated genes

In order to identify potential mediators of miR-150-induced effects, human pulmonary artery endothelial cells (HPAECs) transfected with miR-150 or non-targeting control miRNA were subjected to RNA profiling.

Out of the 13,767 genes identified, 180 genes were significantly upregulated ($p < 0.01$, fold change > 1.5) and 207 were downregulated ($p < 0.01$, fold change < -1.5) by miR-150 (Figure 3A). Heatmap and unsupervised hierarchical clustering of the top 26 differentially expressed genes (with adjusted $p < 0.05$) are shown in Figure 3B. A list of differentially expressed genes is provided in Table S3.

PTEN-like mitochondrial phosphatase (*PTPMT1*), a mitochondrial protein tyrosine phosphatase essential for cardiolipin biosynthesis, was the most significantly altered gene, showing a 2.5-fold increase in expression (adjusted p value of 5.48×10^{-7}), compared with controls. miRNAs can reduce gene expression by binding to the 3′ UTR of target mRNAs or increase target gene expression by binding to gene promoters.[13] RNAhybrid analysis has identified 70 putative miR-150 predicted binding sites to *PTPMT1*, with free energy ranges between −20.2 and −38.1 kcal/mol. The top minimum free energy (MFE) event (−38.1 kcal/mole) occurred within the promoter region of *PTPMT1* (Figure 3C; Figure S4). Predicted binding of miR-150 to *PTPMT1* and transforming growth factor β1 (*TGFB1*) is illustrated in Figure S4. While previous studies showed an upregulation of mRNAs through miRNA binding to their promoter,[14] this mechanism has been relatively less well investigated, compared to mRNA degradation and translational repression through binding to the 3′ UTR. Delineating specific mechanisms through which miR-150 regulates *PTPMT1* and other gene targets will require further studies. The increase in the expression of *PTPMT1* was validated by qPCR (Figure 3D) and western blotting (Figure S5), and reductions in the expression of other genes identified by RNA sequencing (RNA-seq), including *SERPINE1*, *PERP*, *DUSP5*, *NOTCH3*, and *c-MYB*, were validated by qPCR (Figure S5).

Pathway analysis of miR-150 gene targets showed significant associations with pathways regulating cell proliferation, inflammation, and oxidative metabolism, including NOTCH signaling ($p = 0.029$), cardiolipin biosynthesis ($p = 0.014$), and inositol phosphate signaling ($p = 0.007$) (Figure 3E).

Consistent with the findings *in vitro*, quantification of transcripts by qPCR and RNAscope fluorescent *in situ* hybridization, which allows specific identification of single transcripts,[15] confirmed expression changes of miR-150 target genes (*c-MYB* and *NOTCH3*) in the lungs of miR-150-treated animals (Figures S6 and S7). Heart tissue from miR-150-treated Sugen/hypoxia mice showed significantly reduced expression of markers of cardiac hypertrophy and fibrosis, including TGFB1, alpha-1 type I collagen (Col1a1), and regulator of calcineurin 1 (Rcan1) (Figure S8). In contrast, heart tissues from Sugen/hypoxia miR-150iEC-KO mice showed significantly increased levels of Col1a1, compared with the corresponding wild-type disease controls (Figure S9).

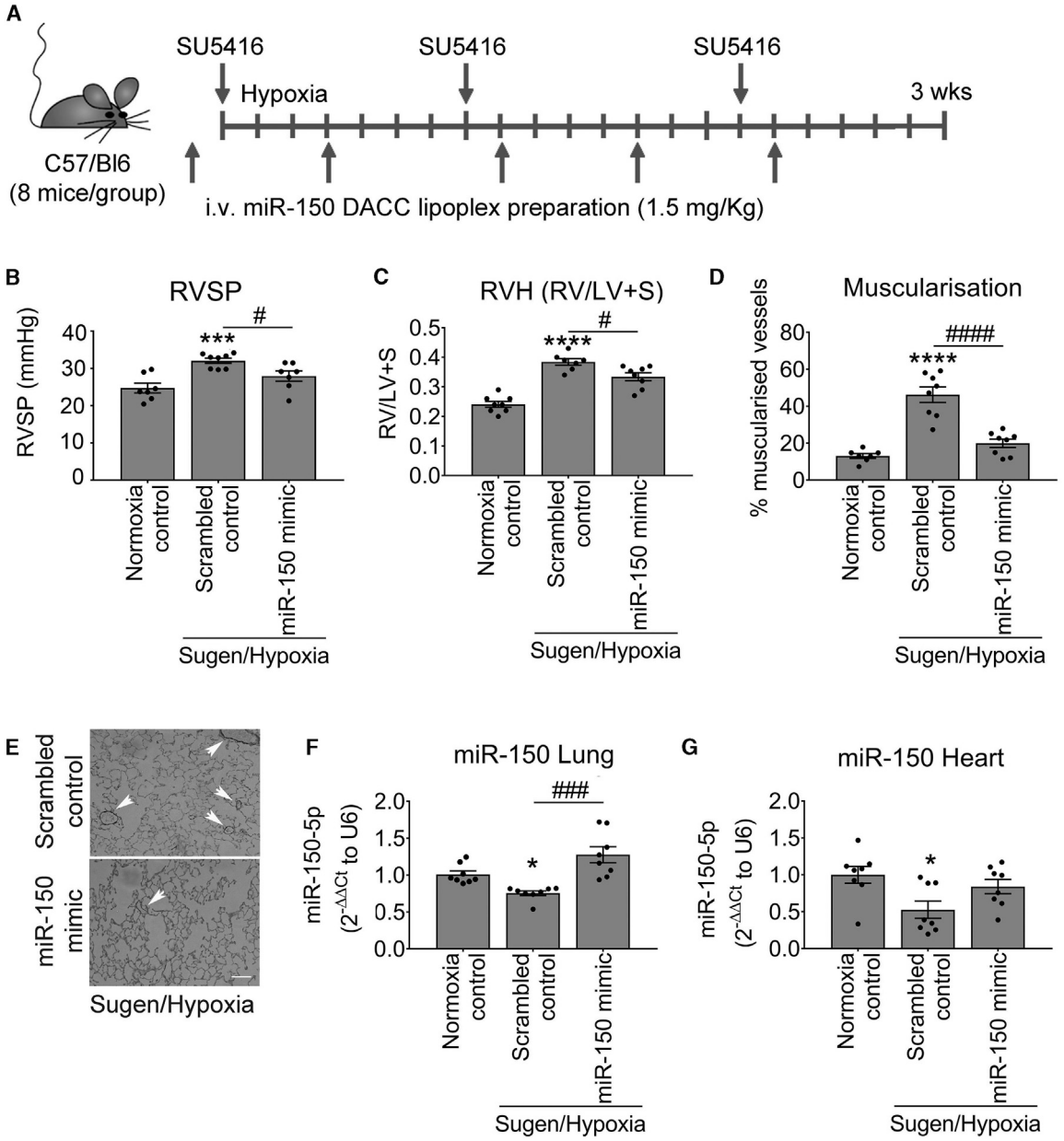

Figure 1. Effect of pulmonary endothelial miR-150 supplementation on development of PH in Sugen/hypoxia mice

(A) Experimental layout. (B–D) Right ventricular systolic pressure (RVSP) (B), right ventricular hypertrophy (RVH; right ventricle to left ventricle + septum ratio [RV/LV+S]) (C), and percentage (D) of muscularized vessels <50 μm in diameter/total number of vessels in the lungs of normoxia control mice and Sugen/hypoxia mice treated with scrambled control or miR-150 mimic delivered by intravenous (i.v.) administration of DACC lipoplex, as indicated. (E) Representative images of α-SMA staining in lung sections from Sugen/hypoxia mice treated with scrambled control or miR-150 mimic. (F and G) miR-150 expression in lung and heart, as indicated; fold change of normoxia control. *$p < 0.05$, **$p < 0.005$, ***$p < 0.001$, ****$p < 0.0001$, comparisons with normoxia control; $^{\#}p < 0.05$, $^{\#\#\#}p < 0.001$, $^{\#\#\#\#}p < 0.0001$, comparisons with scrambled control (by one-way ANOVA with a Tukey's post-test.). Bars are means ± SEM. n = 8 mice/group.

PTPMT1 mediates homeostatic effects of miR-150

In order to study the regulatory role of miR-150 in endothelial cell responses, HPAECs were transfected with miR-150 mimic or miR-150 inhibitor. Changes in the intracellular miR-150 levels were confirmed by qPCR (Figure 4A). Transfection efficiency evaluated with the Cy5-labeled miR negative control was ∼85% (Figure S10). Supplementation of miR-150 markedly attenuated endothelial cell apoptosis, hypoxia-induced cell proliferation, and nuclear factor κB (NF-κB)

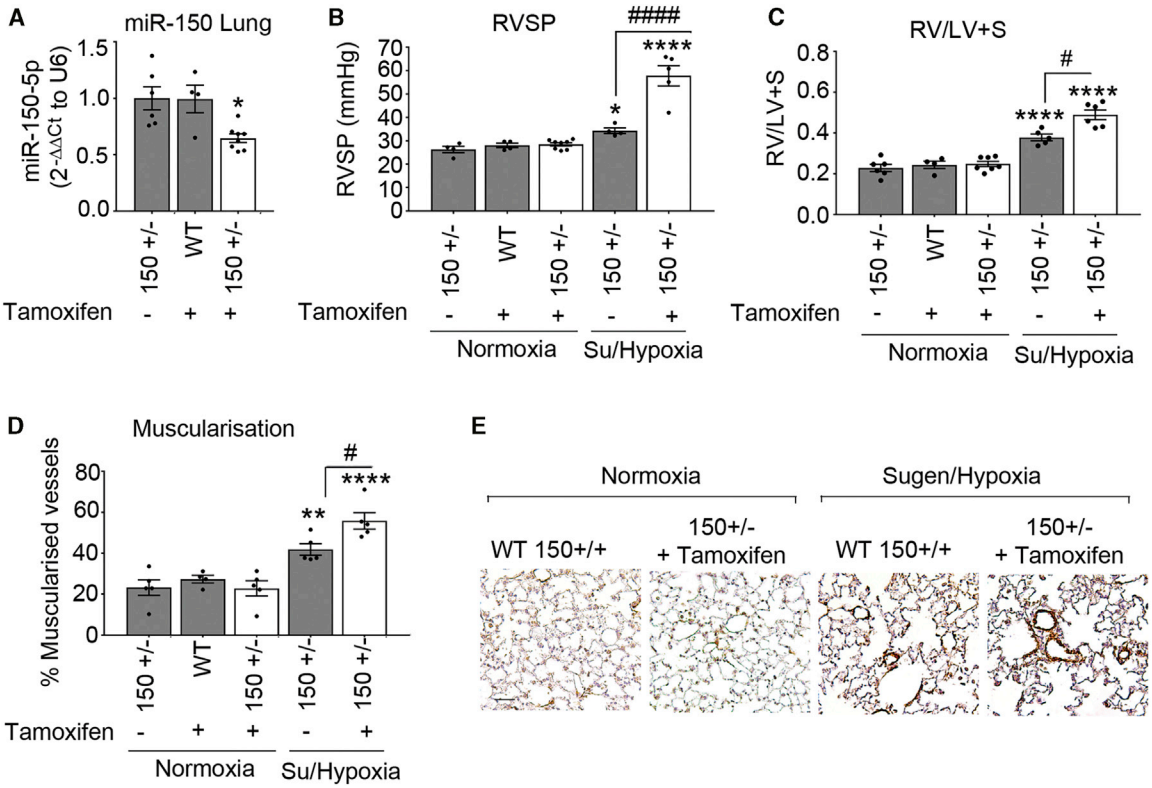

Figure 2. Effect of endothelial miR-150 deletion on development of PH in Sugen/hypoxia mice

(A) Effect of tamoxifen administration on miR-150 levels in lungs of wild-type (WT) ($150^{+/+}$) and miR-150iEC-HTKO mice ($150^{+/-}$). Data are expressed as fold change of normoxia control. (B–D) RVSP (B), RV/LV+S (C), and percentage (D) of muscularized vessels <50 μm in diameter/total number of vessels in the lungs of normoxia wild-type control (+ tamoxifen), normoxia miR-$150^{+/-}$ control (without tamoxifen), and Sugen/hypoxia miR-$150^{+/-}$ mice with and without tamoxifen, as indicated. In (A)–(D), open bars mark miR-150-deficient animals. (E) Representative images of α-SMA staining. Scale bar, 25 μm. *$p < 0.05$, **$p < 0.005$, ****$p < 0.0001$, comparisons with normoxia control; $^{\#}p < 0.05$, $^{\#\#\#\#}p < 0.0001$, comparisons with miR-$150^{+/-}$ control (by one-way ANOVA with a Tukey's post-test). Bars are means ± SEM. n = 4–8 mice/group.

activation (Figures 4B–4D). In contrast, inhibition of miR-150 markedly augmented endothelial damage and inflammatory activation (Figures 4B–4D).

To see whether manipulation of miR-150 levels in endothelial cells can affect smooth muscle cell proliferation, HPAECs and human pulmonary artery smooth muscle cells (HPASMCs) were seeded on the opposite sides of a porous membrane in Transwell dishes (Figure S11). Endothelial miR-150 overexpression significantly reduced hypoxia-induced proliferation of HPASMCs (Figure S11).

Hypoxic exposure significantly reduced PTPMT1 expression in HPAECs (1.5-fold decrease, $p < 0.01$) and HPASMCs (2.5-fold decrease, $p < 0.001$), compared with normoxic controls (Figure S12). Overexpression and silencing of *PTPMT1* (Figure 4E) mimicked, to a large extent, changes induced by manipulation of miR-150 expression (Figures 4F–4H), suggesting that PTPMT1 acts as a key mediator of the anti-proliferative and anti-inflammatory effects of miR-150 in pulmonary endothelial cells.

miR-150 and PTPMT1 improve mitochondrial function in HPAECs

Energy metabolism constitutes an essential link between cell growth and apoptosis.[16] In order to assess the effect of miR-150 and PTPMT1 on energy metabolism, HPAECs and HPAECs transfected with miR-150 or PTPMT1 were subjected to bioenergetic profiling. The extracellular acidification rate (ECAR), which reflects the level of glycolysis, was not significantly affected by either treatment, but mitochondrial oxygen consumption rate (OCR), reflective of the level of mitochondrial respiration, was significantly elevated in miR-150 and PTPMT1-overexpressing cells (Figures 5A–5C).

The treatment of cells with miR-150 and PTPMT1 significantly reduced mitochondrial proton leak (Figure 5D). As proton leak depicts the protons that migrate into the matrix without producing ATP, a reduction in proton leak indicates an improvement in coupling of substrate oxygen and ATP generation.[17]

Measurement of metabolic potential helps to evaluate the capacity of cells to respond to stress conditions associated with increased energy

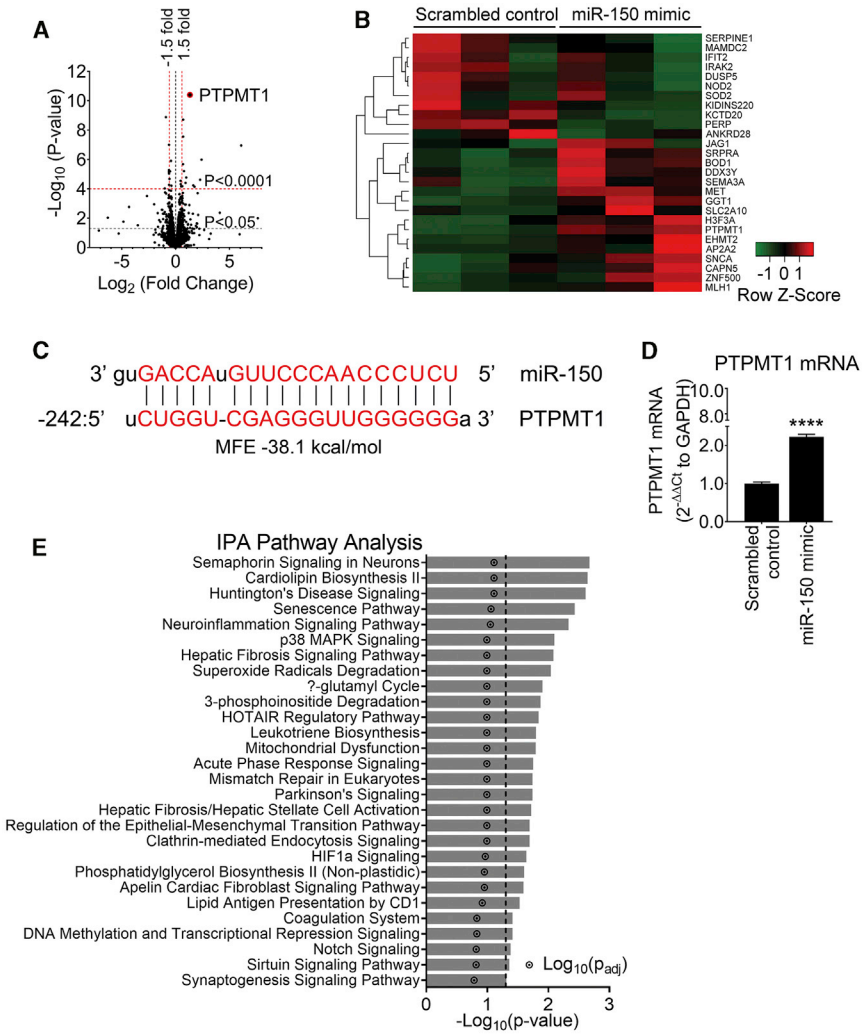

Figure 3. RNA sequencing analysis in miR-150-overexpressing HPAECs shows *PTPMT1* as the most upregulated gene

To identify miR-150 signaling mediators, HPAECs from three different donors were transfected with miR-150 or scrambled control (20 nM) and RNA was extracted for RNA sequencing in three independent experiments. (A) Volcano plot of differentially expressed genes (DEGs). Each point represents the difference in expression (log_2 fold difference) between groups and the associated significance of this change (independent unpaired sample t test). *PTPMT1* is highlighted as the most upregulated gene (fold change of 2.51, p = 3.98×10^{-11}, adjusted p [p-adj] value = 5.48×10^{-7}; n = 3). (B) Heatmap showing 26 most significant genes after multiple test correction using the Benjamini-Hochberg procedure (p-adj < 0.05). Green and red represent downregulation and upregulation, respectively. (C) miR-150 predicted binding sequence with the top minimum free energy (MFE) event (−31.3 kcal/mol) in the promoter (242 bp 5′ upstream) region of the *PTPMT1* gene (chr11:47565430–47573461) using RNAhybrid. (D) PTPMT1 mRNA levels in cells transfected with control miRNA. Bars are mean fold changes of normoxia control ± SEM. n = 5. ****p < 0.0001, comparisons with normoxia control (by unpaired Student's t test). (E) Significantly enriched pathways (p < 0.05) regulated by miR-150; Ingenuity Pathway Analysis (IPA; version 01-12) of top 26 differentially expressed genes in cells transfected with miR-150.

demand via mitochondrial respiration and glycolysis. The results show that miR-150 and PTPMT1 significantly increased mitochondrial metabolic potential measured as fold increase in OCR over basal control levels, while glycolytic metabolic potential in cells remained relatively unaffected (Figures 5E and 5F).

miR-150 and PTPMT1 restore cardiolipin levels in Sugen/hypoxia lung and heart tissues and increase mitochondrial content in human PAH ECFCs

PTPMT1 is a mitochondrial tyrosine kinase, essential for the biosynthesis of cardiolipin, the main phospholipid component of mitochondrial membranes and a key regulator of mitochondrial structure and function.[18,19] We evaluated the effect of miR-150 and PTPMT1 supplementation on cardiolipin levels in lungs and hearts from miR-150-treated Sugen/hypoxia mice, as well as HPAECs and ECFCs from idiopathic PAH (IPAH) patients.

PTPMT1 and cardiolipin levels were significantly reduced in Sugen/hypoxia mice, while miR-150 supplementation restored their expression to the level seen in healthy mice (Figures 6A–6C). Overexpression of PTPMT1 and miR-150 significantly elevated cardiolipin levels in cultured endothelial cells (p < 0.01 and p < 0.05, respectively) (Figure 6D).

Blood-derived ECFCs are often used as surrogates for pulmonary endothelial cells in PAH.[20] qPCR analysis showed that miR-150 and PTPMT1 expressions were markedly reduced in ECFCs from IPAH patients, compared with the cells from healthy individuals (p < 0.01, n = 12–14) (Figures 7A and 7B). IPAH cells also showed a marked (~2-fold, p < 0.05) reduction in cardiolipin levels, which was restored upon treatment with miR-150 and PTPMT1 (Figure 7C).

Reduction in mitochondrial oxidative phosphorylation in PAH is linked with an increase in mitochondrial fragmentation and a reduction in mitochondrial biomass.[5] Accordingly, we observed increased mitochondrial fragmentation and reduced mitochondrial content in ECFCs from IPAH patients, compared with healthy controls (Figures

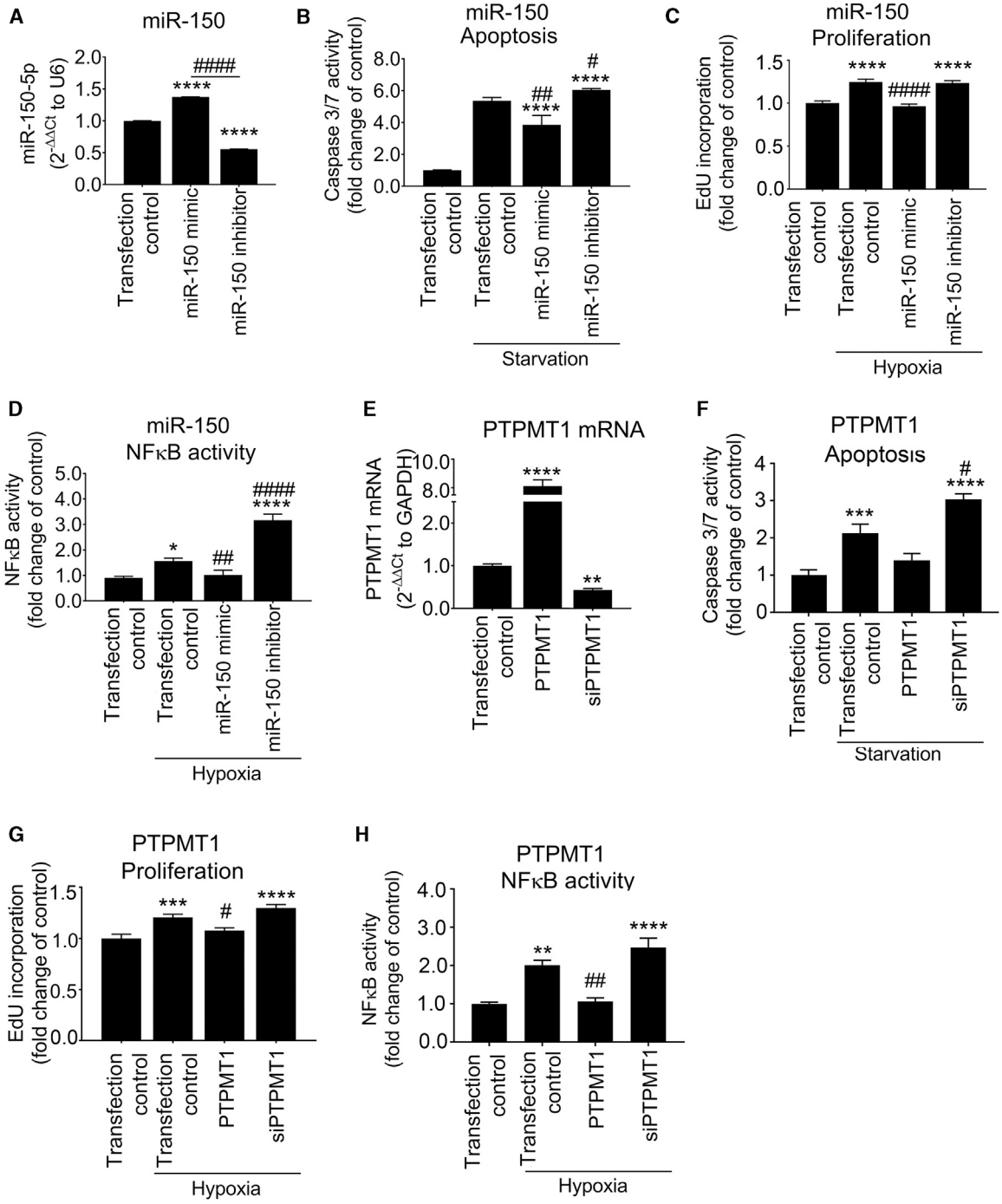

Figure 4. Endothelium-protective effects of miR-150 and PTPMT1

(A–D) Effect of miR-150 mimic and miR-150 inhibitor on (A) miR-150 expression levels in HPAECs, (B) starvation-induced apoptosis (caspase-3/7 activity assay), (C) hypoxia-induced proliferation (EdU incorporation assay), and (D) hypoxia (24 h)-induced NF-κB activity (luciferase reporter assay). (E–H) Effect of PTPMT1 overexpression (PTPMT1) or silencing (siPTPMT1) on (E) PTPMT1 mRNA expression, (F) apoptosis, (G) proliferation, and (H) hypoxia-induced NF-κB activity in HPAECs. In (A), n = 3; in (B)–(H), n = 6. *$p < 0.05$, **$p < 0.001$, ***$p < 0.001$, ****$p < 0.0001$, comparisons with untreated transfection control; $^{\#}p < 0.05$, $^{\#\#}p < 0.001$, $^{\#\#\#\#}p < 0.0001$, comparisons with treated (starvation or hypoxia, as appropriate) transfection controls (one-way ANOVA with a Tukey's post-test). Bars are mean fold changes of transfection control ± SEM.

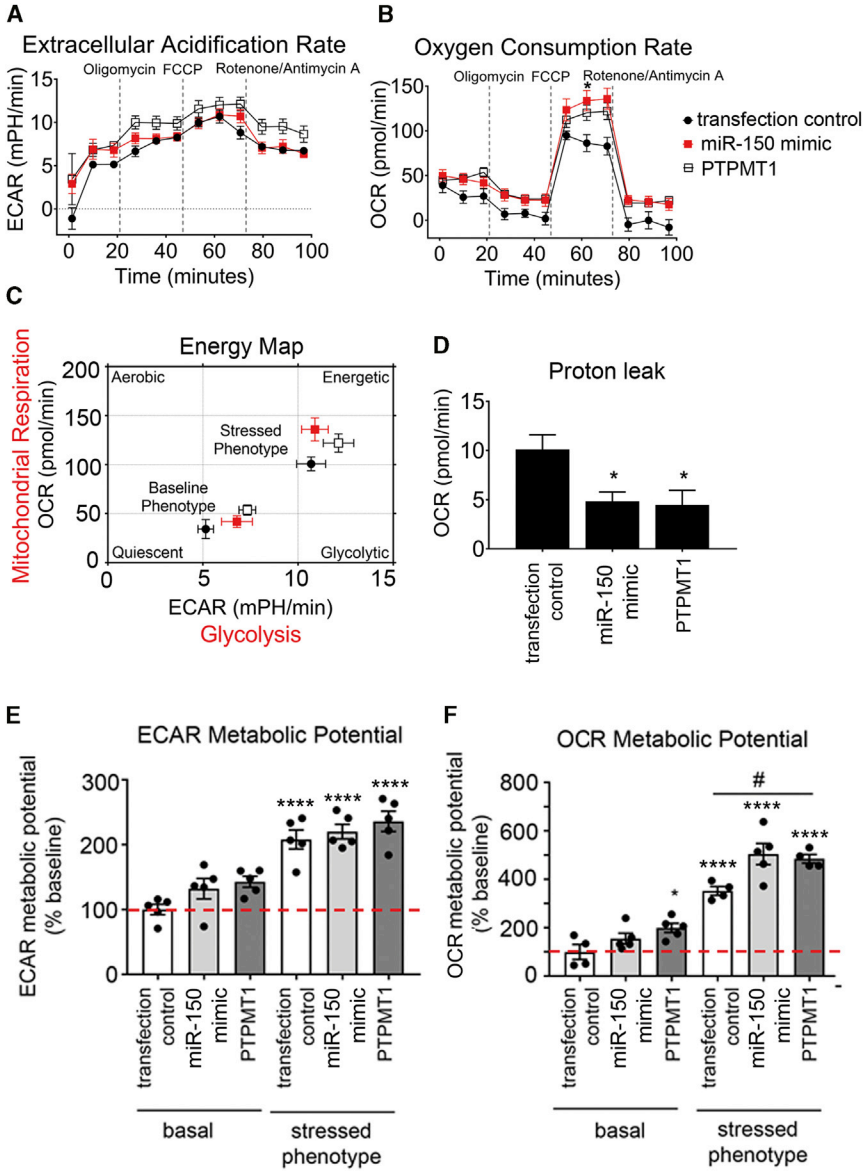

Figure 5. Effect of miR-150 and PTPMT1 on metabolic potential in HPAECs

(A–F) Extracellular acidification rate (ECAR) (A), oxygen consumption rate (OCR) (B), energy map (C), proton leak (D), ECAR metabolic potential (% of basal control) (E), and OCR metabolic potential (% of basal control) (F) in control HPAECs (transfection control) and HPAECs transfected with miR-150 or PTPMT1, as indicated. n = 5. Bars are means ± SEM. *$p < 0.05$, ****$p < 0.0001$, comparison with transfection control (basal); #$p < 0.05$, as indicated (by one-way ANOVA with a Tukey's post-test).

7D–7F). Overexpression of miR-150 and PTPMT1 restored healthy control phenotype in IPAH cells (Figures 7D–7F).

DISCUSSION

This study highlights the key role of endothelial miR-150 in the regulation of pulmonary vascular homeostasis. We show that supplementation of miR-150 reduces expression of markers of inflammation, apoptosis, and fibrosis critical to the pathology of PAH, including c-MYB, NOTCH3, TGF-β and Col1a1, and it enhances mitochondrial metabolic potential via increased expression of PTPMT1, the key regulator of cardiolipin biosynthesis.

Downregulation of miR-150 in pulmonary endothelium and IPAH endothelial cells may result from transcriptional repression by apoptosis-inducer p53,[21] which is highly expressed in endothelial cells in pulmonary hypertensive lung.[22] Hypoxia and inhibition of Krüppel-like factor 2 (KLF-2) and bone morphogenetic protein receptor 2 (BMPR2) are also likely to play contributory roles.[23–26]

RNA sequencing identified *PTPMT1* as a key gene affected by miR-150 overexpression, and functional analysis showed that PTPMT1 has endothelium-protective effects. PTPMT1 is exclusively localized to the inner membrane of mitochondria, with close proximity to electron transport chain complexes and enzymes of the tricarboxylic acid cycle.[19] Interestingly, PTPMT1-ablated cells show a marked decrease in aerobic metabolism, enhancement of glycolysis,[19] and mitochondrial fragmentation,[27] reminiscent of changes seen in PAH.[28] Accordingly, we observed that miR-150 and PTPMT1 supplementation restored mitochondrial content and reduced mitochondrial fragmentation in PAH ECFCs to the level seen in healthy controls.

The effects of PTPMT1 can be linked to its role in the biosynthesis of cardiolipin, a mitochondrial-specific phospholipid regulating mitochondrial membrane integrity and function. Interaction with cardiolipin is required for optimal activity of several inner mitochondrial membrane proteins, including the enzyme complexes of the electron transport chain and ATP production.[18]

miR-150 and PTPMT1 may reduce maladaptive right ventricular remodeling by augmentation of glucose oxidation and prevention of capillary rarefaction.[29] In addition to the increased PTPMT1 levels, miR-150-treated Sugen/hypoxia mice showed reduced expression of cardiac hypertrophy and the fibrosis markers Col1a1, TGFB1, and Rcan1.[30] Reduction in Col1a1 expression is likely to be mediated by direct targets of miR-150, c-MYB, Sp1, or β_3 integrin.[31,32] miR-150 interaction with TGFB1 can potentially occur through multiple locations, with the top predicted

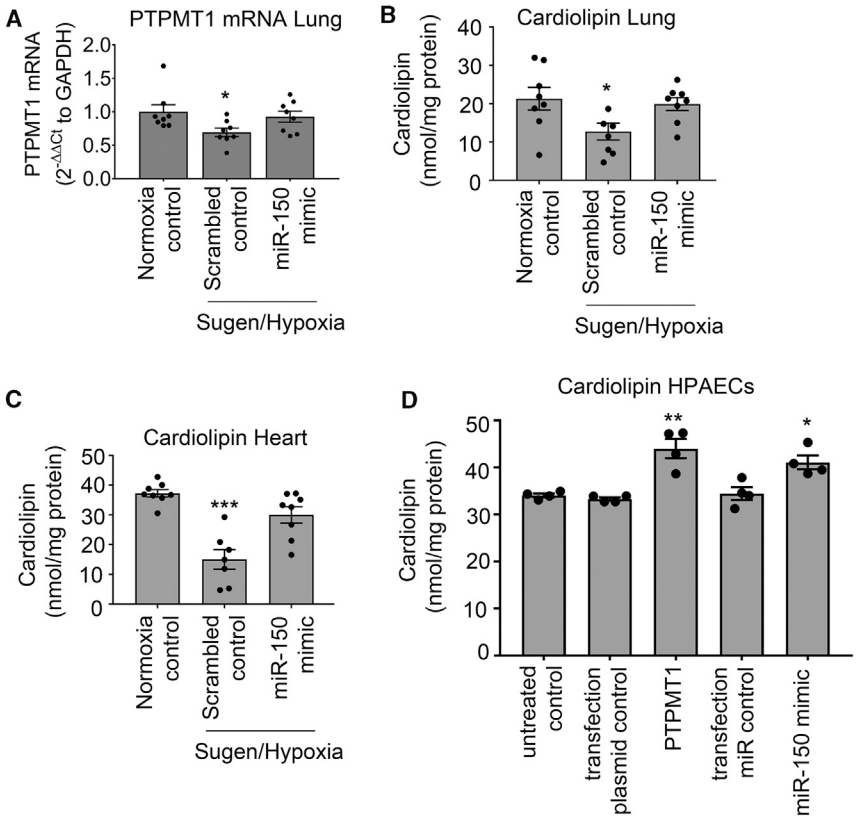

Figure 6. miR-150 and PTPMT1 modulate cardiolipin levels in tissues and cells

(A–C) Lung PTPMT1 mRNA (A), lung cardiolipin (B), and heart cardiolipin (C) levels in control and DACC/miR-150-treated Sugen/hypoxia mice, as indicated. (D) Cardiolipin levels in control HPAECs and HPAECs transfected with miR-150 and PTPMT1, as indicated. In (A), data are expressed as fold change of normoxia control. Bars are mean of ± SEM. *p < 0.05, **p < 0.01, ***p < 0.001, comparison with transfection control (by one-way ANOVA with a Tukey's post-test). n = 4–8.

site within the first intron of TGFB1. Interestingly, TGF-β signaling can also block miR-150 expression,[31,33] suggesting the existence of a feedback regulatory mechanism. Further studies are required to establish the precise nature of miR-150 interactions with its target genes.

Endothelial apoptosis, increased ROS generation and reduction in mitochondrial cardiolipin contribute to right ventricular failure in PAH.[34,35] Electron leak is the major causative factor for production of mitochondrial superoxide, and hence the reduction in mitochondrial proton leak by PTPMT1 may account for the beneficial effects of miR-150 treatment.

Anti-remodeling effects of miR-150 are likely to result from the cumulative changes in expression of multiple genes. Besides PTPMT1, other signaling mediators, including c-MYB, NOTCH3, activin receptors 1 and 2, and matrix metalloproteinases, are likely to play a role. c-MYB stimulates cell migration, increases recruitment of endothelial progenitor cells,[36] and promotes cardiac hypertrophy and fibrosis.[37] NOTCH3 is a marker and predictor of PAH, and its blockade is sufficient to reverse experimental PAH.[38,39] Consistently, we observed contemporaneous, opposing changes in the expression of miR-150 and its targets, c-MYB and NOTCH3, in human cells and lung tissues from PAH mice. While the overall effect of DACC-mediated miR-150 supplementation was beneficial, it showed a mild hepatotoxic effect, possibly as a result of liposomal clearance by the liver. While miRNAs can pleiotropically target multiple disease pathways and miRNA drugs start to enter clinical medicine, it is important to consider their potential off-target effects.[40] Therefore, organ-specific drug delivery and new platforms evaluating toxicity and therapeutic efficacy of miRNA candidates ought to be developed. The use of other pre-clinical models of PAH in addition to Sugen/hypoxia mice would be needed for the full evaluation of miR-150 and PTPMT1-based therapies.

To summarize, we show that reduction in endothelial miR-150 levels has adverse effects on pulmonary hemodynamics in PAH mice, while endothelium-targeted delivery of miR-150 is protective. In addition to the anti-proliferative and anti-fibrotic actions of miR-150, activation of PTPMT1-cardiolipin signaling by this miRNA may facilitate adaptation of lung and heart to high energy demand in stress conditions induced by mechanical workload, hypoxia, or inflammation.

MATERIALS AND METHODS

Animal experiments

All studies were conducted in accordance with UK Home Office Animals (Scientific Procedures) Act 1986. To induce PAH, 8- to 12-week-old C57BL/6 male mice (20 g; Charles River Laboratories, UK) were injected subcutaneously with Sugen (SU5416; 20 mg/kg) and housed in hypoxia (10% O_2) for 3 weeks (n = 8/group).[41] mirVana hsa-miR-150-5p (ID MC10070) mimic or scrambled miRNA control (Ambion) in complex with DACC lipoplex preparation (Silence Therapeutics, London, UK)[9] was administered intravenously once every fourth day at 1.5 mg/kg/day for 3 weeks, on five occasions to PAH mice and normoxic healthy controls. The first injection was given 1 day before Sugen/hypoxia administration. At 3 weeks, the mice were anesthetized by intraperitoneal injection of ketamine/Domitor (75 mg/kg + 1 mg/kg). The development of PAH was verified as previously described.[41]

Mice with inducible, conditional, endothelium-specific deletion of miR-150 were obtained by crossing floxed miR-150 mice (stock *Mir150*^{tm1Mtm}/Mmjax mice from Jackson Laboratory) on a

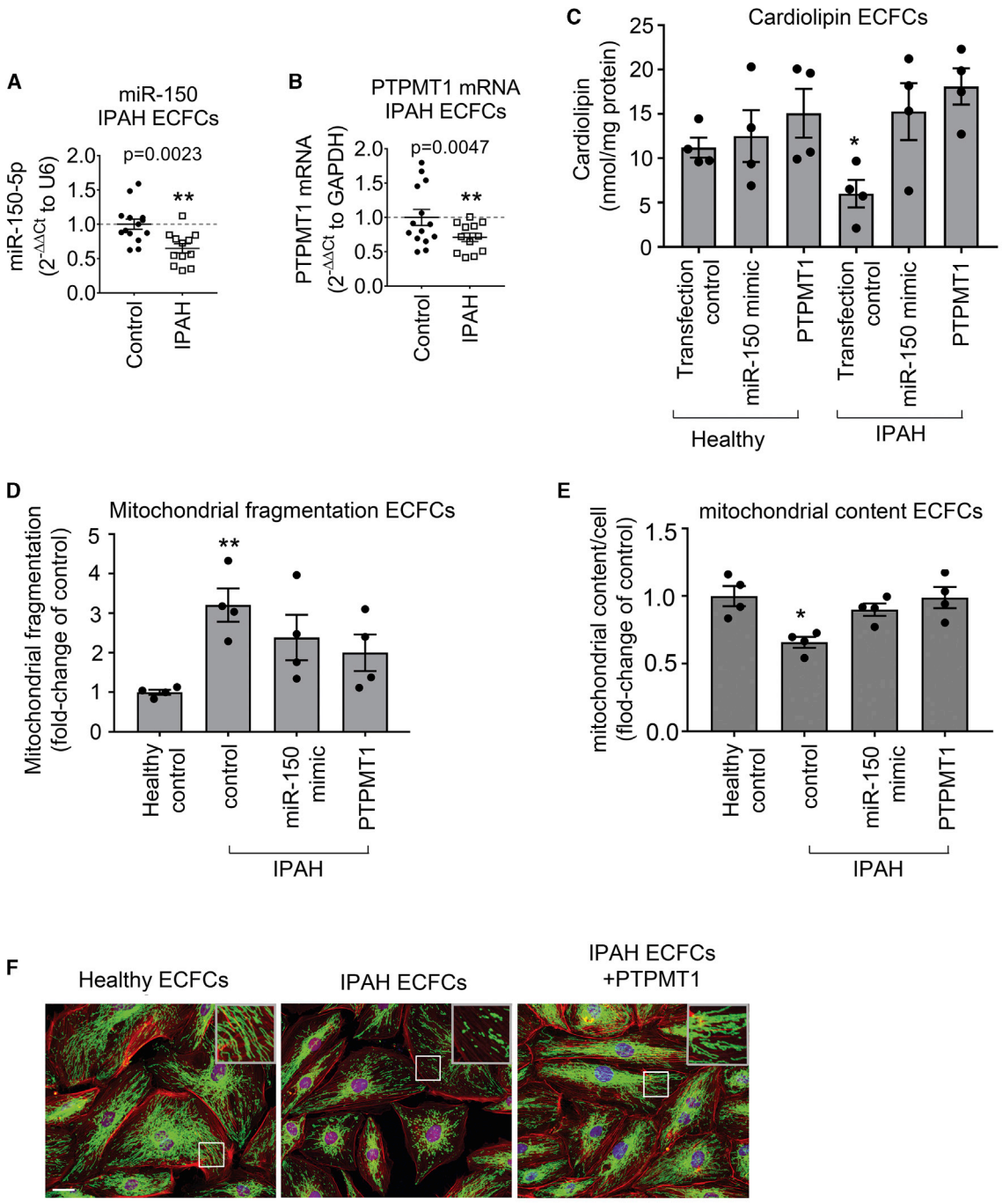

Figure 7. miR-150, PTPMT1, and cardiolipin levels and mitochondrial biogenesis in IPAH ECFCs

(A and B) miR-150 (A) and PTPMT1 (B) expression levels in ECFCs from healthy individuals and IPAH patients (fold change of control). (C–E) Cardiolipin levels (C), mitochondrial fragmentation (D), and mitochondrial content (mitochondrial coverage/cell) (E) in ECFCs treated, as indicated. (F) Representative images of mitochondrial fragmentation in healthy and IPAH ECFCs. Inset in the top right corner is an enlarged image of the boxed area. Mitochondria were immunolabeled with fluorescein isothiocyanate (FITC) (green) and F-actin with tetramethylrhodamine isothiocyanate (TRITC)-phalloidin (red). Scale bar, 10 μm. Data are expressed as means ± SEM. *$p < 0.05$, **$p < 0.01$, comparison with healthy control. In (A) and (B), n = 12–14; in (C)–(E), n = 4.

C57BL/6 background with C57BL/6 mice carrying tamoxifen-inducible Cre recombinase under the control of the Cdh5 promoter (Cdh5(PAC)-iCreERT2).[42] Deletion of miR-150 in miR-150$^{fl/fl}$/Cdh5(PAC)-iCreERT2 mice (referred to as miR-150iEC-KO) induced by tamoxifen was confirmed by PCR.

A detailed description of experimental procedures is available in the Supplemental materials and methods.

AST activity assay

An AST assay - (MAK055, Sigma-Aldrich, Darmstadt, Germany) was performed on frozen mouse liver tissues, according to the manufacturer's guidelines.

RNAscope

For formalin-fixed, paraffin-embedded lung sections, an RNAscope multiplex fluorescent reagent kit v2 (Advanced Cell Diagnostics, Newark, CA, USA) and a TSA cyanine 3 & 5, tetramethylrhodamine (TMR), fluorescein evaluation kit system (PerkinElmer, Waltham, MA, USA) were used according to the manufacturers' protocols.

A detailed description of experimental procedures is available in the Supplemental materials and methods.

Cell culture

HPAECs and HPASMCs were cultured as previously described.[41] Cells were exposed to hypoxia (5% CO_2, 2% O_2) for 24–72 h.

A detailed description of non-contact cell culture and cell treatments is available in the Supplemental materials and methods.

Blood-derived human endothelial cells and human lung samples

All investigations were conducted in accordance with the Declaration of Helsinki. Venous blood samples were obtained with the approval of the Brompton Harefield & NHLI and Hammersmith Hospitals Research Ethics Committees, and informed written consent was received from healthy volunteers (n = 14) and patients with IPAH (n = 12). Human ECFCs were derived from peripheral blood samples as previously described.[41] Clinical information and experimental procedures are provided in the Supplemental materials and methods.

Cell transfection

Detailed descriptions of transfection procedures and cell treatments are available in the Supplemental materials and methods.

Quantitative real-time PCR

RNA was extracted from cultured cells or tissue using a Monarch total RNA miniprep kit (New England Biolabs, Ipswich, MA, USA). Input RNA was reverse transcribed using a LunaScript RT supermix kit (New England Biolabs) or a TaqMan miRNA reverse transcription kit (Thermo Fisher Scientific, Waltham, MA, USA) and a custom multiplex RT primer pool in a SimpliAmp thermal cycler (Applied Biosystems, Foster City, CA, USA) according to the manufacturers' instructions. A list of TaqMan miRNA and gene expression assays and additional methodological information are available in the Supplemental materials and methods.

Western blotting

Protein levels of PTPMT1 and β-actin in HPAECs transfected with scrambled miRNA and miR-150 mimic obtained 24 h post-transfection were determined by western blotting. Blots were probed with mouse monoclonal anti-β-actin (Sigma-Aldrich, A1978; 1:3,000), mouse monoclonal anti-PTPMT1 (Santa Cruz Biotechnology, sc-390901; 1:500) and secondary antibodies, and horseradish peroxidase (HRP)-linked sheep anti-mouse immunoglobulin G (IgG) (GE Healthcare, NAG31V; 1:1,000). The relative intensity of the immunoreactive bands was determined by densitometry using ImageJ software (National Institutes of Health, https://imagej.nih.gov/ij/), and PTPMT1 expression was normalized to β-actin.

RNA sequencing and identification of signaling mediators of miR-150

Next-generation RNA sequencing was carried out as previously described.[24] Genes were considered differentially expressed when the adjusted p value was greater than 0.05 and there was at least a 1.5-fold change in expression. miRNA target prediction was carried out with TargetScan Human, miRecords, and Ingenuity Expert Findings. Gene enrichment was carried out using Ingenuity Pathway Analysis (IPA, version 01-12, QIAGEN, Hilden, Germany).

The RNA sequencing data generated and analyzed during this study are available in the BioProject repository at the following link: https://www.ncbi.nlm.nih.gov/bioproject/PRJNA645887 (BioProject ID PRJNA645887; BioSamples SAMN15518378, SAMN15518379, SAMN5518380, SAMN15518381, SAMN15518382, and SAMN15518383; SRA accession nos. SRR12210268, SRR12210267, SRR12210266, SRR12210265, and SRR12210264).

RNAhybrid[43] was used to identify the MFE hybridization of the mature miR-150 (MIMAT0000451) sequence against the DNA sequence within a 2-kbp window inclusive of the gene body for *PTPMT1* (chr11:47563600–47575461) and *TGFB1* (chr19:41328324–41355922). A maximum of 100 hits per target and a maximum MFE threshold of −20 with approximate p values estimated from the 3utr_human for the target sequence were applied.

Measurement of cell apoptosis, proliferation, and inflammatory activation

A 5-ethynyl-2′-deoxyuridine (EdU) proliferation assay, NF-κB activity, and caspase-3/7 apoptosis assays were carried out as previously described.[41] Additional details are provided in the Supplemental materials and methods.

Seahorse bioenergetics assay

OCRs and ECARs were measured in a Seahorse extracellular flux analyzer using XF24 (Seahorse Bioscience, North Billerica, MA,

USA) and with a Seahorse XF mito stress test kit (Agilent Technologies, Santa Clara, CA, USA, 103015-100).

Immunostaining

A detailed description of experimental procedures is available in the Supplemental materials and methods.

Cardiolipin measurement

Quantification of cardiolipin was carried out with cardiolipin assay kit (BioVision, Milpitas, CA, USA, K944-100).

Mitochondrial fragmentation count and mitochondrial content

Mitochondrial fragmentation (area taken by mitochondrial particles <2 μm in length)[44] and total mitochondrial coverage (area taken by all mitochondria) were determined in confocal images using NIP2 image software.[45] A detailed description of experimental procedures is available in the Supplemental materials and methods.

Statistical analysis

All experiments were performed at least in triplicate, and measurements were taken from distinct samples. Data are presented as mean ± SEM. Normality of data distribution was assessed with a Shapiro-Wilk test in GraphPad Prism 7.03. Comparisons between two groups were made with a Student's t test or Mann-Whitney's U test, whereas three or more groups were compared by use of ANOVA with a Tukey's post hoc test or Kruskal-Wallis test with Dunn's post hoc test, as appropriate. Statistical significance was accepted at $p < 0.05$.

SUPPLEMENTAL INFORMATION

Supplemental Information can be found online at https://doi.org/10.1016/j.omtn.2020.10.042.

ACKNOWLEDGMENTS

We thank the staff of the Imperial NIHR/Imperial Clinical Research Facility, Hammersmith Hospital (London, UK) and Dr. John Wharton (NHLI) for help in acquiring cells from IPAH patients. We also thank Prof. Anna Randi and Dr. Graeme Birdsay (NHLI, Imperial College London) for providing Cdh5(PAC)-iCreERT2 mice. This research was supported by PhD studentships from the Government of Saudi Arabia (to M.M.A.) and by British Heart Foundation project grant PG/16/4/31849.

AUTHOR CONTRIBUTIONS

G.R., K.B.J., V.B.A.-S., M.M.A., C.C.M., A.H.O., J.E., U.S., and B.W.-S. performed *in vitro* experiments and analyzed data; K.B.J., G.R., and V.B.A.-S. performed *in vitro* and *in vivo* experiments, immunohistochemistry, and analyzed data; M.M.A. provided analysis of mitochondrial fragmentation; M.R.W. critically analyzed the manuscript; C.M. analyzed RNA sequencing data; M.R.W. provided IPAH patient data; and B.W.-S. secured funding, performed experiments, and wrote the manuscript.

DECLARATION OF INTERESTS

This work involved the collaboration of B.W.-S. with Silence Therapeutics (London, UK), who provided DACC/miRNA preparations. The remaining authors declare no competing interests.

REFERENCES

1. Schermuly, R.T., Ghofrani, H.A., Wilkins, M.R., and Grimminger, F. (2011). Mechanisms of disease: pulmonary arterial hypertension. Nat. Rev. Cardiol. *8*, 443–455.
2. Ranchoux, B., Harvey, L.D., Ayon, R.J., Babicheva, A., Bonnet, S., Chan, S.Y., Yuan, J.X., and Perez, V.J. (2018). Endothelial dysfunction in pulmonary arterial hypertension: an evolving landscape (2017 Grover Conference Series). Pulm. Circ. *8*, 2045893217752912.
3. Freund-Michel, V., Khoyrattee, N., Savineau, J.P., Muller, B., and Guibert, C. (2014). Mitochondria: roles in pulmonary hypertension. Int. J. Biochem. Cell Biol. *55*, 93–97.
4. Paulin, R., and Michelakis, E.D. (2014). The metabolic theory of pulmonary arterial hypertension. Circ. Res. *115*, 148–164.
5. Culley, M.K., and Chan, S.Y. (2018). Mitochondrial metabolism in pulmonary hypertension: beyond mountains there are mountains. J. Clin. Invest. *128*, 3704–3715.
6. Negi, V., and Chan, S.Y. (2017). Discerning functional hierarchies of microRNAs in pulmonary hypertension. JCI Insight *2*, e91327.
7. Rhodes, C.J., Wharton, J., Boon, R.A., Roexe, T., Tsang, H., Wojciak-Stothard, B., Chakrabarti, A., Howard, L.S., Gibbs, J.S., Lawrie, A., et al. (2013). Reduced microRNA-150 is associated with poor survival in pulmonary arterial hypertension. Am. J. Respir. Crit. Care Med. *187*, 294–302.
8. Gubrij, I.B., Pangle, A.K., Pang, L., and Johnson, L.G. (2016). Reversal of microRNA dysregulation in an animal model of pulmonary hypertension. PLoS ONE *11*, e0147827.
9. Fehring, V., Schaeper, U., Ahrens, K., Santel, A., Keil, O., Eisermann, M., Giese, K., and Kaufmann, J. (2014). Delivery of therapeutic siRNA to the lung endothelium via novel Lipoplex formulation DACC. Mol. Ther. *22*, 811–820.
10. Abdul-Salam, V.B., Russomanno, G., Chien-Nien, C., Mahomed, A.S., Yates, L.A., Wilkins, M.R., Zhao, L., Gierula, M., Dubois, O., Schaeper, U., et al. (2019). CLIC4/Arf6 pathway. Circ. Res. *124*, 52–65.
11. Tanaka, K., Nanbara, S., Tanaka, T., Koide, H., and Hayashi, T. (1988). Aminotransferase activity in the liver of diabetic mice. Diabetes Res. Clin. Pract. *5*, 71–75.
12. Sercombe, L., Veerati, T., Moheimani, F., Wu, S.Y., Sood, A.K., and Hua, S. (2015). Advances and challenges of liposome assisted drug delivery. Front. Pharmacol. *6*, 286.
13. Vaschetto, L.M. (2018). miRNA activation is an endogenous gene expression pathway. RNA Biol. *15*, 826–828.
14. Zhang, Y., Fan, M., Zhang, X., Huang, F., Wu, K., Zhang, J., Liu, J., Huang, Z., Luo, H., Tao, L., and Zhang, H. (2014). Cellular microRNAs up-regulate transcription via interaction with promoter TATA-box motifs. RNA *20*, 1878–1889.
15. Wang, F., Flanagan, J., Su, N., Wang, L.C., Bui, S., Nielson, A., Wu, X., Vo, H.T., Ma, X.J., and Luo, Y. (2012). RNAscope: a novel in situ RNA analysis platform for formalin-fixed, paraffin-embedded tissues. J. Mol. Diagn. *14*, 22–29.
16. Mason, E.F., and Rathmell, J.C. (2011). Cell metabolism: an essential link between cell growth and apoptosis. Biochim. Biophys. Acta *1813*, 645–654.
17. Cheng, J., Nanayakkara, G., Shao, Y., Cueto, R., Wang, L., Yang, W.Y., Tian, Y., Wang, H., and Yang, X. (2017). Mitochondrial proton leak plays a critical role in pathogenesis of cardiovascular diseases. Adv. Exp. Med. Biol. *982*, 359–370.
18. Dudek, J. (2017). Role of cardiolipin in mitochondrial signaling pathways. Front. Cell Dev. Biol. *5*, 90.
19. Shen, J., Liu, X., Yu, W.M., Liu, J., Nibbelink, M.G., Guo, C., Finkel, T., and Qu, C.K. (2011). A critical role of mitochondrial phosphatase Ptpmt1 in embryogenesis reveals a mitochondrial metabolic stress-induced differentiation checkpoint in embryonic stem cells. Mol. Cell. Biol. *31*, 4902–4916.

20. Duong, H.T., Comhair, S.A., Aldred, M.A., Mavrakis, L., Savasky, B.M., Erzurum, S.C., and Asosingh, K. (2011). Pulmonary artery endothelium resident endothelial colony-forming cells in pulmonary arterial hypertension. Pulm. Circ. *1*, 475–486.

21. Ghose, J., and Bhattacharyya, N.P. (2015). Transcriptional regulation of microRNA-100, -146a, and -150 genes by p53 and NFκB p65/RelA in mouse striatal STHdh^{Q7}/Hdh^{Q7} cells and human cervical carcinoma HeLa cells. RNA Biol. *12*, 457–477.

22. Wang, Z., Yang, K., Zheng, Q., Zhang, C., Tang, H., Babicheva, A., Jiang, Q., Li, M., Chen, Y., Carr, S.G., et al. (2019). Divergent changes of p53 in pulmonary arterial endothelial and smooth muscle cells involved in the development of pulmonary hypertension. Am. J. Physiol. Lung Cell. Mol. Physiol. *316*, L216–L228.

23. Hergenreider, E., Heydt, S., Tréguer, K., Boettger, T., Horrevoets, A.J., Zeiher, A.M., Scheffer, M.P., Frangakis, A.S., Yin, X., Mayr, M., et al. (2012). Atheroprotective communication between endothelial cells and smooth muscle cells through miRNAs. Nat. Cell Biol. *14*, 249–256.

24. Sindi, H.A., Russomanno, G., Satta, S., Abdul-Salam, V.B., Jo, K.B., Qazi-Chaudhry, B., Ainscough, A.J., Szulcek, R., Jan Bogaard, H., Morgan, C.C., et al. (2020). Therapeutic potential of KLF2-induced exosomal microRNAs in pulmonary hypertension. Nat. Commun. *11*, 1185.

25. Chen, M., Shen, C., Zhang, Y., and Shu, H. (2017). MicroRNA-150 attenuates hypoxia-induced excessive proliferation and migration of pulmonary arterial smooth muscle cells through reducing HIF-1α expression. Biomed. Pharmacother. *93*, 861–868.

26. Eichstaedt, C.A., Song, J., Viales, R.R., Pan, Z., Benjamin, N., Fischer, C., Hoeper, M.M., Ulrich, S., Hinderhofer, K., and Grünig, E. (2017). First identification of *Krüppel-like factor 2* mutation in heritable pulmonary arterial hypertension. Clin. Sci. (Lond.) *131*, 689–698.

27. Zhang, J., Guan, Z., Murphy, A.N., Wiley, S.E., Perkins, G.A., Worby, C.A., Engel, J.L., Heacock, P., Nguyen, O.K., Wang, J.H., et al. (2011). Mitochondrial phosphatase PTPMT1 is essential for cardiolipin biosynthesis. Cell Metab. *13*, 690–700.

28. Dasgupta, A., Wu, D., Tian, L., Xiong, P.Y., Dunham-Snary, K.J., Chen, K.H., Alizadeh, E., Motamed, M., Potus, F., Hindmarch, C.C.T., and Archer, S.L. (2020). Mitochondria in the pulmonary vasculature in health and disease: oxygen-sensing, metabolism, and dynamics. Compr. Physiol. *10*, 713–765.

29. Ryan, J.J., and Archer, S.L. (2014). The right ventricle in pulmonary arterial hypertension: disorders of metabolism, angiogenesis and adrenergic signaling in right ventricular failure. Circ. Res. *115*, 176–188.

30. Voelkel, N.F., Quaife, R.A., Leinwand, L.A., Barst, R.J., McGoon, M.D., Meldrum, D.R., Dupuis, J., Long, C.S., Rubin, L.J., Smart, F.W., et al.; National Heart, Lung, and Blood Institute Working Group on Cellular and Molecular Mechanisms of Right Heart Failure (2006). Right ventricular function and failure: report of a National Heart, Lung, and Blood Institute working group on cellular and molecular mechanisms of right heart failure. Circulation *114*, 1883–1891.

31. Zheng, J., Lin, Z., Dong, P., Lu, Z., Gao, S., Chen, X., Wu, C., and Yu, F. (2013). Activation of hepatic stellate cells is suppressed by microRNA-150. Int. J. Mol. Med. *32*, 17–24.

32. Honda, N., Jinnin, M., Kira-Etoh, T., Makino, K., Kajihara, I., Makino, T., Fukushima, S., Inoue, Y., Okamoto, Y., Hasegawa, M., et al. (2013). miR-150 down-regulation contributes to the constitutive type I collagen overexpression in scleroderma dermal fibroblasts via the induction of integrin β3. Am. J. Pathol. *182*, 206–216.

33. Davoodian, P., Ravanshad, M., Hosseini, S.Y., Khanizadeh, S., Almasian, M., Nejati Zadeh, A., and Esmaiili Lashgarian, H. (2017). Effect of TGF-β/smad signaling pathway blocking on expression profiles of miR-335, miR-150, miR-194, miR-27a, and miR-199a of hepatic stellate cells (HSCs). Gastroenterol. Hepatol. Bed Bench *10*, 112–117.

34. Rawat, D.K., Alzoubi, A., Gupte, R., Chettimada, S., Watanabe, M., Kahn, A.G., Okada, T., McMurtry, I.F., and Gupte, S.A. (2014). Increased reactive oxygen species, metabolic maladaptation, and autophagy contribute to pulmonary arterial hypertension-induced ventricular hypertrophy and diastolic heart failure. Hypertension *64*, 1266–1274.

35. Saini-Chohan, H.K., Dakshinamurti, S., Taylor, W.A., Shen, G.X., Murphy, R., Sparagna, G.C., and Hatch, G.M. (2011). Persistent pulmonary hypertension results in reduced tetralinoleoyl-cardiolipin and mitochondrial complex II + III during the development of right ventricular hypertrophy in the neonatal pig heart. Am. J. Physiol. Heart Circ. Physiol. *301*, H1415–H1424.

36. Wang, W., Li, C., Li, W., Kong, L., Qian, A., Hu, N., Meng, Q., and Li, X. (2014). miR-150 enhances the motility of EPCs in vitro and promotes EPCs homing and thrombus resolving in vivo. Thromb. Res. *133*, 590–598.

37. Deng, P., Chen, L., Liu, Z., Ye, P., Wang, S., Wu, J., Yao, Y., Sun, Y., Huang, X., Ren, L., et al. (2016). MicroRNA-150 inhibits the activation of cardiac fibroblasts by regulating c-Myb. Cell. Physiol. Biochem. *38*, 2103–2122.

38. Havrda, M.C., Johnson, M.J., O'Neill, C.F., and Liaw, L. (2006). A novel mechanism of transcriptional repression of p27^{kip1} through Notch/HRT2 signaling in vascular smooth muscle cells. Thromb. Haemost. *96*, 361–370.

39. Li, X., Zhang, X., Leathers, R., Makino, A., Huang, C., Parsa, P., Macias, J., Yuan, J.X., Jamieson, S.W., and Thistlethwaite, P.A. (2009). Notch3 signaling promotes the development of pulmonary arterial hypertension. Nat. Med. *15*, 1289–1297.

40. Hanna, J., Hossain, G.S., and Kocerha, J. (2019). The potential for microRNA therapeutics and clinical research. Front. Genet. *10*, 478.

41. Wojciak-Stothard, B., Abdul-Salam, V.B., Lao, K.H., Tsang, H., Irwin, D.C., Lisk, C., Loomis, Z., Stenmark, K.R., Edwards, J.C., Yuspa, S.H., et al. (2014). Aberrant chloride intracellular channel 4 expression contributes to endothelial dysfunction in pulmonary arterial hypertension. Circulation *129*, 1770–1780.

42. Wang, Y., Nakayama, M., Pitulescu, M.E., Schmidt, T.S., Bochenek, M.L., Sakakibara, A., Adams, S., Davy, A., Deutsch, U., Lüthi, U., et al. (2010). Ephrin-B2 controls VEGF-induced angiogenesis and lymphangiogenesis. Nature *465*, 483–486.

43. Rehmsmeier, M., Steffen, P., Hochsmann, M., and Giegerich, R. (2004). Fast and effective prediction of microRNA/target duplexes. RNA *10*, 1507–1517.

44. Farrand, L., Kim, J.Y., Im-Aram, A., Suh, J.Y., Lee, H.J., and Tsang, B.K. (2013). An improved quantitative approach for the assessment of mitochondrial fragmentation in chemoresistant ovarian cancer cells. PLoS ONE *8*, e74008.

45. Martinez, K., and Cupitt, J. (2005). VIPS—a highly tuned image processing software architecture. In Proceedings of the IEEE International Conference on Image Processing 2005 (IEEE), p. II-574, https://doi.org/10.1109/ICIP.2005.1530120.

OMTN, Volume *23*

Supplemental Information

miR-150-PTPMT1-cardiolipin signaling in pulmonary arterial hypertension

Giusy Russomanno, Kyeong Beom Jo, Vahitha B. Abdul-Salam, Claire Morgan, Jens Endruschat, Ute Schaeper, Ahmed H. Osman, Mai M. Alzaydi, Martin R. Wilkins, and Beata Wojciak-Stothard

SUPPLEMENTAL MATERIAL

"Mir-150-PTPMT1-Cardiolipin signaling in Pulmonary Arterial Hypertension"

Giusy Russomanno, Kyeong Beom Jo, Vahitha B. Abdul-Salam, Claire Morgan, Jens Endruschat, Ute Schaeper, Ahmed H. Osman, Mai M. Alzaydi, Martin R. Wilkins & Beata Wojciak-Stothard*.

Animal experiments

All studies were conducted in accordance with UK Home Office Animals (Scientific Procedures) Act 1986. All animals were randomly allocated to groups, and all personnel involved in data collection and analysis (haemodynamics and histopathologic measurements) were blinded to the treatment status of each animal. Only weight-and age-matched males were included for experimentation as, in contrast to the human clinical studies, most animal studies have shown that female sex and estrogen supplementation have a protective effect against PAH.

To induce PAH, 8-12 weeks old C57/BL male mice (20 g; Charles River, UK) were injected subcutaneously with Sugen (SU5416; 20mg/kg), suspended in 0.5% [w/v] carboxymethylcellulose sodium, 0.9% [w/v] sodium chloride, 0.4% [v/v] polysorbate 80, 0.9% [v/v] benzyl alcohol in deionized water once/week. Control mice received only vehicle. Mice were either housed in normal air or placed in a normobaric hypoxic chamber (10% O_2) for 3 weeks (n= 8/group).

mirVana hsa-miR-150-5p (ID MC10070) mimic or scrambled miRNA control (Ambion) in complex with DACC lipoplex preparation (Silence Therapeutics)[1] was administered intravenously via tail vein injection once every fourth day at 1.5 mg/kg/day for 3 weeks, on 5 occasions. The first injection was given 1 day before Sugen/hypoxia administration. At 3 weeks, the mice were anaesthetised by intraperitoneal injection of Ketamine/Dormitor (75 mg/kg + 1 mg/kg).

In addition, to follow the distribution of liposomal cargo, a single intravenous injection of fluorescently labelled DACC/siRNA-Cy3 (2.8 mg/kg body weight) in healthy mice was performed. Localization of the fluorescently-labelled RNA in paraffin sections of lung, heart, kidney, spleen and liver taken 4 and 24 hours post-injection, was analysed with fluorescent confocal imaging.

To produce mice with inducible conditional endothelium-specific deletion of miR-150, floxed miR-150 mice (STOCK Mir150^{tm1Mtm}/Mmjax mice from Jackson Laboratories) C57/Bl6 background were crossed with C57/Bl6 mice carrying tamoxifen-inducible Cre recombinase under the control of the Cdh5 promoter (Cdh5(PAC)-iCreERT2[2]. Following tamoxifen administration, efficient Cre-recombinase deletion of miR-150 was confirmed by PCR in miR-150$^{fl/fl}$/Cdh5(PAC)-iCreERT2 mice (henceforth referred to as miR-150iEC-KO).

Weaned mice were ear-notched and samples were incubated in lysis buffer (100 mM Tris HCl pH 8.5, 5 mM EDTA, 200 mM NaCl, 0.2% SDS, 0.14 mg/mL Proteinase K, Ambion^{TM}) for 2 hours at 55°C under agitation (700 rpm). Samples were then vortexed and pelleted at 14,000 rpm for 10 minutes. Supernatant was transferred to a new DNase-free tube and DNA was precipitated in isopropanol (20 minutes incubation at RT). DNA was pelleted at 14,000 x g for 10 minutes, supernatant was discarded and the DNA pellet was air dried and then resuspended in 100 µL of DNase-free water.

PCR reactions were performed using REDTaq® ReadyMix™ PCR Reaction Mix (Sigma-Aldrich, cat. R2523) with the primers listed in Supplemenrary Table S1 (500 nM of each) in a SmplyAmp^{TM} Thermal Cycler (Applied Biosystems). All primers were purchased from Sigma-Aldrich.

Thermocycling conditions for miR-150 followed the Jackson Laboratory's instructions (www.jax.org): 2 min at 94°C, then 20 s at 94°C, 15 s at 65°C, 10 s at 68°C, for 10 cycles, 15

s at 94°C, 15 s at 60°C, 10 s at 72°C, for 28 cycles, and a last step of 2 min at 72°C. For Cre genotyping, thermocycling conditions were as follows: 3 min at 94°C, then 30 s at 94°C, 30 s at 70°C, 60 s at 72°C, for 32 cycles, and a last step of 10 min at 72°C.

All PCR products were separated on a 2% agarose gel, visualized using GelRed Nucleic Acid Gel Stain (Thermo Fisher Scientific, cat. NC0017761), and size was estimated with comparison to a DNA mass ladder (GeneRuler 100 bp DNA Ladder, Thermo Fisher Scientific, cat. SM0243).

At 6 weeks of age, miR-150^{fl}/Cdh5(PAC)-iCreERT2 mice were injected intraperitoneally with 100 µL of 5 mg/mL tamoxifen (Sigma, cat. no. T5648) or vehicle (12.5% vol/vol ethanol in peanut oil) for 5 consecutive days[3]. Littermate wild-type animals were used as control. Two weeks after tamoxifen injection, mice were injected with Sugen and housed in normal air or hypoxia for 3 weeks (n=4-8/group).

The development of PAH was verified by measuring right ventricular systolic pressure (RVSP), right ventricular hypertrophy (assessed as the right ventricle to left ventricle/septum ratio - RV/LV+S), and muscularisation of small intrapulmonary arteries, as previously described[4]. RVSP was measured via direct cardiac puncture using a closed-chest technique in the spontaneously breathing, anesthetized animal. Pressure measurements were repeated three times and the mean value used. Data were collected by Power Lab Data Acquisition system (AD Instruments) and analysed using LabChart 8 software (AD Instruments) by an investigator blinded to the treatment group.

The right lung lobe was harvested and snap frozen in liquid nitrogen or placed in RNAlater® RNA Stabilization Solution for RNA isolation. The left lobe was inflation-fixed (10% formaldehyde in PBS), embedded in paraffin, and sectioned for histology. The heart and liver were collected and snap frozen or placed in RNAlater®. Transverse formalin-fixed lung sections

were stained with an anti-smooth muscle actin antibody (DAKO M0851) or Verhoeff's van Gieson stain (EVG) to visualise elastic lamina. Pulmonary vascular remodelling (muscularisation of small intrapulmonary arteries) was determined by counting all muscularised vessels with a diameter smaller than 50 μm in each lung section and expressed as a % of all (muscularised + non-muscularised) vessels. Counting was performed by two observers blinded to treatment.

In situ hybridization

In situ hybridization was carried out on paraffin lung sections of untreated mice and Sugen/hypoxia mice (n=3, 5 weeks hypoxia) using miRCURY LNA™ microRNA ISH Optimization kit (Exiqon, cat no 339459). Negative control: LNA™ scrambled microRNA probe, double DIG labelled (40 nM); Positive controls: LNA™ U6snRNA probe, 5'DIG-labeled (1 nM), LNA™ microRNA223 probe, double DIG labelled (40 nM, labels myeloid, granulocytic and monocytic cell lineages in the hematopoietic system). LNA™ microRNA150 probe double DIG labelled (40 nM) was used to study changes in miR-150 levels. Hybridization temperature: 54°C. The sections were incubated with sheep anti-DIG antibody (1:200, Roche Applied Science; cat. no 1333 089), biotinylated donkey anti-sheep antibody (1:200, Sigma, cat no. AP184B), streptavidin-peroxidase conjugate (1:200), followed by DAB/hematoxylin staining. A detailed protocol can be found in miRCURY LNA miRNA Detection Probes Handbook – Qiagen.

RNAscope®

For formalin-fixed, paraffin-embedded lung sections, RNAscope® Multiplex Fluorescent Reagent Kit v2 (Advanced Cell Diagnostics) and TSATM Cyanine 3 & 5, TMR, Fluorescein Evaluation Kit System (PerkinElmer) were used according to manufactures' protocols[5].

Briefly, tissue sections in 5-µm thickness were baked in a dry oven (Agilent G2545A Hybridization Oven, Agilent Technologies) for 1 hour at 60°C, and deparaffinised in xylene, followed by dehydration in 100% ethanol. Tissue sections were then incubated with RNAscope® Hydrogen Peroxide for 10 minutes at room temperature. After washing twice with distilled water, manual target retrieval was performed boiling the sections (100°C to 103°C) in 1X Target Retrieval Reagents using a hot plate for 15 minutes. Slides were then rinsed in deionized water, 100% ethanol, and incubated with RNAscope® Protease Plus at 40°C for 30 minutes in a HybEZ hybridization oven (Advanced Cell Diagnostics, PN 321710/321720). Hybridization with target probes (Mm-Myb-C1, NM_001198914.1; Mm-Notch3-C2, NM_025576.2) was carried out incubating the slides at 40°C for 2 hours. Two different probes/channels (C1-C2) were multiplexed. After washing twice with Wash Buffer, slides were stored overnight in 5x SSC buffer (0.75M NaCl, 0.075M sodium citrate). The following day, the slides were incubated at 40°C with the following reagents: Amplifier 1 (30 min), Amplifier 2 (30 min), Amplifier 3 (15 min); HRP-C1 (15 min), TSA® Plus fluorophore for channel 1 (fluorescein, PerkinElmer; 1:1000; 30 min), HRP blocker (15 min); HRP-C2 (15 min), TSA® Plus fluorophore for channel 2 (cyanine 3, PerkinElmer; 1:1000; 30 min), HRP blocker (15 min). After each hybridization step, slides were washed three times with Wash Buffer at room temperature.

RNAscope hybridisation was combined with immunofluorescence[5, 6]. Tissue was blocked for 1 hour at room temperature with 3% normal horse serum (Vector Laboratories) in 1X PBS containing 0.1% bovine serum albumin (Sigma-Aldrich), and 0.01% sodium azide (Sigma-Aldrich), and then incubated with polyclonal rabbit antibody raised against human von

Willebrand Factor (1:500; A0082, Dako), at 4°C overnight. After three washes in PBS, slides were incubated with FITC-labelled Goat Anti-Rabbit antibody (1:100; 111-095-003, Jackson ImmunoResearch Inc.) for 30 minutes at RT. Following immunostaining, tissues were mounted in Vectashield with DAPI and examined under a fluorescent confocal microscope (Leica, TCS SP5, Leica Biosystems, Bretton, Peterborough).

Cell culture

Human pulmonary artery endothelial cells (HPAECs, Promocell, C-12241) were cultured in endothelial cell growth medium 2 (ECGM2; PromoCell, C-22111) and human pulmonary artery smooth muscle cells (HPASMCs, Lonza, CC-2581) in smooth muscle cell growth medium 2 (SMCGM2, PromoCell, C-22062), as previously described [4]. In some experiments, the cells were exposed to hypoxia (5% CO_2, 2% O_2) for 18-72 hours.

For non-contact co-culture of HPAECs and HPASMCs, Transwell dishes with 0.4 μm pore polyester membrane inserts (Scientific Laboratory Supplies, UK) were used. HPAECs were seeded into the fibronectin-coated top chambers and cultured in complete ECGM2 medium, whereas HPASMCs were seeded at the bottom of the plate and cultured in complete SMCGM2 for 24 h. The two cell types were then washed with PBS, combined together and co-cultured in endothelial cell basal medium supplemented with 10% FBS (Sigma-Aldrich, F7524), and selected components of ECGM2 supplement pack (PromoCell, C-22111): EGF (2.5 ng/L), FGF (10 ng/L), IGF (20 ng/L) with 1% penicillin and streptomycin.

Blood-derived human endothelial cells and human lung samples

All investigations were conducted in accordance with the Declaration of Helsinki. Venous blood samples were obtained with the approval of the Brompton Harefield & NHLI and

Hammersmith Hospitals Research Ethics committees and informed written consent from healthy volunteers (n=14) and patients with idiopathic PAH (IPAH, n=12). Participants were identified by number. Human endothelial colony forming cells (ECFCs) were derived from peripheral blood samples as previously described [4]. Clinical information is shown in Table S2.

Cell Transfection

Briefly, HPAECs were left untreated (control) or were transfected with control miRNA (non-targeting transfection control; Ambion Life Technologies, 4464076) at 20 nmol/L, or miRVana^{TM} has-miR-150-5p, (4464066 Assay ID MC10070;), miRVana^{TM} miRNA inhibitor, (4464084, Assay ID MH10070), both at 20 nmol/L, or control siRNA (non-targeting negative control siRNA; Invitrogen, 4390843) at 10 nmol/L, or siPTPMT1 (4392420 Assay ID s229946) at 10 nmol/L, using Lipofectamine RNAiMAX in antibiotic-free media, following manufacturer's instruction. After 24 hours, the media were changed and cells were exposed to hypoxia for 24-72 hours. Alternatively, on the following day, the untransfected and transfected cells were starved for 9 hours before caspase 3/7 assay. Human pcDNA PTPMT1, NM_175732.2 (clone OHu11042; 2B Scientific Ltd. Upper Heyford, UK) was transfected into HPAECs with Lipofectamine RNAiMAX at 2ng/well in a 24-well dish, as recommended by the manuafacturer. Transfection efficiency was measured by the uptake of Cy3™ Dye-Labeled Pre-miR Negative Control (AM17120; Thermo Fisher Scientific) and quantitative real-time PCR (RT-qPCR). All experiments were performed 24 hours after transfection. Transfected cells were exposed to hypoxia (2% O_2, 5% CO_2), serum and growth factor depletion or inflammatory cytokines. Cell proliferation and NFκB activity assays were carried out 72 and 48 hours post-transfection, respectively.

RNA Extraction

RNA was extracted from cultured cells or tissue (~10 mg) stored in RNALater® using Monarch® Total RNA Miniprep Kit (New England BioLabs). For maximal RNA recovery, tissues was mechanically homogenized using a Kinematica™ Polytron™ PT 1300 D and incubated at 55°C for 5 minutes with Proteinase K following manufacturer's instructions. To remove any residual DNA that may affect downstream applications, an On-Column DNase I digestion was also performed. RNA concentration and purity was evaluated using NanoDrop 2000 spectrophotometer (Thermo Scientific). The A260/230 and A260/280 ratios were used to assess the presence of contaminants. RNA was then stored at -80°C for later experiments.

Real-time quantitative PCR

Input RNA (50-100 ng/µL) was reverse-transcribed using LunaScript® RT SuperMix Kit (New England BioLabs) or TaqMan MicroRNA Reverse Transcription Kit (Thermo Fisher Scientific) and custom Multiplex RT Primer pool in a SimpliAmp™ Thermal Cycler (Applied Biosystems), according to the manufacturer's instructions. The multiplex RT primer pool consisted of primers for miR-150-5p and U6 (Thermo Fisher Scientific). No-template samples where included as negative controls.

TaqMan® miRNA Assays for hsa-miR-150-5p (Assay ID 000473), and U6 snRNA (Assay ID 001973), and TaqMan® Gene Expression Assays for PTPMT1 (Hs00378514_m1, Mm00458631_m1), SERPINE1 (Hs00167155_m1), PERP (Hs00953482_g1), DUSP5 (Hs00244839_m1), c-MYB (Hs00920556_m1, Mm00501741_m1), NOTCH3 (Hs01128537_m1, Mm01345646_m1), Col1a1 (Mm00801666_g1), Rcan1 (Mm01213406_m1), Tgfb1 (Mm01178820_m1), and GAPDH (Hs02786624_g1, Mm99999915_g1; all Thermo Fisher Scientific), were used to perform quantitative PCR

(qPCR). No-template samples were included as negative controls and all PCRs were performed in triplicate. The reaction was performed on a QuantStudio 12K Flex Real-Time PCR System (Applied Biosystems). Data were analysed using QuantStudio 12K Flex Software version 1.2 (Applied Biosystems). For relative quantification, the data were analysed using the $2^{-\Delta\Delta Ct}$ method, where U6 snRNA and GAPDH were used as endogenous normalization controls for miR-150 and gene expression, respectively.

RNA-Sequencing and identification of signaling mediators of miR-150

10µl of RNA (250-300 ng/µl) extracted from cells transfected with miR-150 mimic or scrambled control in three independent experiments, were sent in to Imperial BRC Genomics Facility (Imperial College of London, UK) for next-generation RNA-sequencing RNA quality and quantity were assessed using an Agilent 2100 Bioanalyzer (Agilent Technologies) and a Qubit 4 Fluorometer (Thermo Fisher Scientific). RNA libraries were prepared using TruSeq® Stranded mRNA HT Sample Prep Kit (Illumina Inc., USA) according to the manufacturer's protocol as previously described[6]. Libraries were run over 4 lanes (2 x 100 bp) on a HiSeq 2500 (Illumina Inc.) resulting in an average of 34.4 million reads per sample. Sequence data was de-multiplexed using bcl2fastq2 Conversion Software v2.18 (Illumina Inc.) and quality analysed using FastQC (http://www.bioinformatics.babraham.ac.uk/projects/fastqc). Transcripts from paired-end stranded RNA-Seq data were quantified with Salmon v 0.8.2 using hg38 reference transcripts[7, 8]. Count data was normalised to accommodate known batch effects and library size using DESeq2[9]. Pairwise differential expression analysis was performed based on a model using the negative binomial distribution and p-values were adjusted for multiple test correction using the Benjamini-Hochberg procedure[10]. Genes were considered differentially expressed if the adjusted p-value was greater than 0.05 and there was at least a 1.5 fold change in expression. miRNA target prediction was carried out with TargetScan Human, miRecords and Ingenuity

Expert Findings. Gene enrichment was carried out using Ingenuity Pathway Analysis (IPA, Qiagen).

Accession numbers for RNA sequencing data will be provided upon provisional acceptance of the manuscript.

Caspase 3/7 apoptosis assay

Cells were incubated in serum- and growth factor-depleted medium for 9 hours to induce apoptosis. Apoptosis was measured using Cell Meter^{TM} Caspase 3/7 Activity Apoptosis Assay Kit (AAT Bioquest, ABD-22796). Fluorescence intensity was analysed in Glomax^{TM} luminometer at Ex/Em = 490/525 nm.

NFκB luciferase reporter assay

NFκB activity was measured in luciferase reporter assay [4] in the Glomax^{TM} luminometer.

EdU Proliferation Assay

The EdU Cell Proliferation Assay Kit (EdU-594, EMD Millipore Corp, USA, 17-10527) was used to measure cell proliferation, according to the manufacturer's protocol. Proliferation of ECFCs from healthy individuals and IPAH patients was evaluated in serum-reduced, growth factor-depleted media.

Seahorse Bioenergetics Assay

Oxygen consumption (OCR) and extracellular acidification rates (ECAR) were measured in Seahorse Extracellular Flux Analyzer using XF24 (Seahorse Bioscience, North Billerica, MA) and Seahorse XF Mito Stress Test Kit (Agilent, 103015-100). 4 x 10^4 cells were plated into each well prior to the assay. Cells cultured on the Seahorse XF Cell Culture microplates were left untreated or were transfected with miR-150 or PTPMT1, as previously described for 24h overexpression. The sensor cartridge was hydrated at 37°C in Seahorse XF Calibrant overnight in a non-CO_2 incubator.

The assay medium was prepared by supplementing Seahorse XF Base Medium with 1mM pyruvate (S8636), 2mM glutamate and glucose (G8540) and 10mM glucose (G8769), warming it up to 37°C and adjusting pH to 7.4. All compounds were warmed up to room temperature. 1μM oligomycin, 1μM FCCP and 0.5μM rotenone/antimycin A provided with the kit were loaded into the appropriate ports of hydrated sensor cartridge. The cells were incubated with assay medium for 1h before Seahorse XF Mito Stress Test. OCR and ECAR were normalized to the protein concentration.

Immunostaining

Immunostaining of paraffin embedded lung sections was carried out as previously described[4].

To stain mitochondria, HPAECs cultured on Thermanox® Plastic Coverslips (13 mm) were washed twice in PBS, fixed in 4% formaldehyde for 15 min at room temperature, washed in PBS and permeabilised with 0.1% Triton X-100 (Sigma-Aldrich, 234729) in PBS for 10 min. The cells were then rinsed with PBS, blocked in 10% normal goat serum (Vector Laboratories, S-1000) for 1 h and incubated with mouse anti-mitochondria antibodies (Abcam, ab92824) diluted 1:100 in PBS in 5% BSA in a humidified chamber overnight. Cells were then rinsed 3 times with PBS and incubated with FITC-Goat Anti-Mouse IgG (Jackson ImmunoResearch

Inc.,115-095-003; 1:200) with tetramethylrhodamine (TRITC)-phalloidin (1 μg/mL; Sigma-Aldrich, UK, P1951) for 1h. Following immunostaining, cells were mounted in Vectashield Antifade Mounting Medium containing nuclear stain DAPI (Vector Laboratories, H-1200) and examined under the fluorescent confocal microscope (Leica, TCS SP5, Leica Biosystems, Bretton, Peterborough).

Cardiolipin measurement

Quantification of cardiolipin in cells and tissues was carried out with Cardiolipin Assay Kit (BioVision, cat. K944-100), according to the manufacturer's instructions.

Mitochondrial fragmentation count and mitochondrial content

Mitochondrial were immunolabelled, as described above. Mitochondrial fragmentation (area taken by mitochondrial particles < 2μm in length)[11] and total mitochondrial coverage (area taken by all mitochondria) were determined using NIP2 image software [12] . The 2μm cut-off size was optimal[11] in selection of mitochondria unassociated with mitochondrial network. Briefly, the acquired images were filtered (median), thresholded, and binarized to identify individual mitochondrial segments and score the total area of fragmented mitochondria. This value was normalized to the total mitochondrial area (in pixels) in each cell, to define the individual cell's MFC. For each intervention 20 randomly selected cells were analysed in 3 separate experiments [13].

Table S1. Sequences of specific primers used for mouse genotyping.

Gene	Primer	Sequence	Amplicon length (bp)

MIR150	Forward	5’-GTTCAAGCAGATCATGATACTCAA-3’	304 (WT) - 396 (Mutant)
	Reverse	5’-GTCCTGGGACAGAGCAAAGATT-3’	
Cre	Forward	5’-GCCTGCATTACCGGTCGATGCAACGA-3’	720 (Mutant)
	Reverse	5’-GTGGCAGATGGCGCGGCAACACCATT-3’	

Table S2. Demographic and clinical features of patients and healthy volunteers. Venous blood samples were obtained with local ethics committee approval and informed written consent from healthy volunteers and patients with idiopathic PAH (IPAH). Data represented as median (range).

		Control (n=14)	IPAH (n=12)
Male/Females		3/11	1/11
Age (years)		30.0 (23.0 - 45.0)	38.33 (27.0 - 67.0)
Time from diagnosis (months)		-	13.0 (0.1 - 60.0)
mPAP (mmHg)		-	65.0 (28.0 - 94.0)
Six minute walk distance (m)		-	396.0 (300.0 – 540.0)
WHO Functional Class	I	-	1
	II	-	3
	III	-	5
	IV	-	3
Treatment naïve		-	2
Warfarin		-	4
Calcium Antagonists		-	1
ER Antagonists		-	7
PDE5 Inhibitors		-	8
Prostanoids		-	4
Statins		-	0

mPAP, mean Pulmonary Arterial Pressure; ER, Estrogen-Receptor; PDE5, Phosphodiesterase type 5.

Table S3. Top 26 differentially expressed genes (DEG, adjusted p-value<0.05) in miR-150 transfected HPAECs (RNA-Sequencing).

Gene ID	Log_2FC	Adj p-value	Entrez Gene Name	Location	Type(s)
PTPMT1	1.329	5.48×10^{-7}	protein tyrosine phosphatase, mitochondrial 1	Cytoplasm	phosphatase
PERP	-0.904	8.88×10^{-6}	PERP, TP53 apoptosis effector	Plasma Membrane	other
H3F3A	0.698	8.92×10^{-6}	H3 histone family member 3A	Nucleus	other
DDX3Y	0.699	9.52×10^{-5}	DEAD-box helicase 3, Y-linked	Cytoplasm	enzyme
AP2A2	6.084	2.54×10^{-4}	adaptor related protein complex 2 alpha 2 subunit	Cytoplasm	transporter
IFIT2	-0.616	2.54×10^{-4}	interferon induced protein with tetratricopeptide repeats 2	Cytoplasm	other
EHMT2	2.405	2.00×10^{-3}	euchromatic histone lysine methyltransferase 2	Nucleus	transcription regulator
SERPINE1	-0.430	2.13×10^{-3}	serpin family E member 1	Extracellular Space	other
SNCA	0.686	3.24×10^{-3}	synuclein alpha	Cytoplasm	enzyme
ANKRD28	-0.620	7.30×10^{-3}	ankyrin repeat domain 28	Cytoplasm	other
IRAK2	-0.522	7.31×10^{-3}	interleukin 1 receptor associated kinase 2	Plasma Membrane	kinase
MLH1	0.773	7.31×10^{-3}	mutL homolog 1	Nucleus	enzyme
KIDINS220	-0.627	7.42×10^{-3}	kinase D interacting substrate 220	Nucleus	transcription regulator
MAMDC2	-0.613	9.04×10^{-3}	MAM domain containing 2	Extracellular Space	other
ZNF500	0.986	0.0156	zinc finger protein 500	Nucleus	other
DUSP5	-0.572	0.0179	dual specificity phosphatase 5	Nucleus	phosphatase
SLC2A10	2.272	0.0195	solute carrier family 2 member 10	Plasma Membrane	transporter
JAG1	0.457	0.0214	jagged 1	Extracellular Space	growth factor
CAPN5	0.917	0.0284	calpain 5	Cytoplasm	peptidase
SRPRA	0.468	0.0329	SRP receptor alpha subunit	Cytoplasm	other
KCTD20	-0.611	0.0349	potassium channel tetramerization domain containing 20	Cytoplasm	other
SEMA3A	1.637	0.0366	semaphorin 3A	Extracellular Space	other
SOD2	-0.392	0.0369	superoxide dismutase 2	Cytoplasm	enzyme
BOD1	0.624	0.0377	biorientation of chromosomes in cell division 1	Nucleus	other
MET	0.522	0.0378	MET proto-oncogene, receptor tyrosine kinase	Plasma Membrane	kinase
GGT1	1.759	0.0379	gamma-glutamyltransferase 1	Plasma Membrane	enzyme

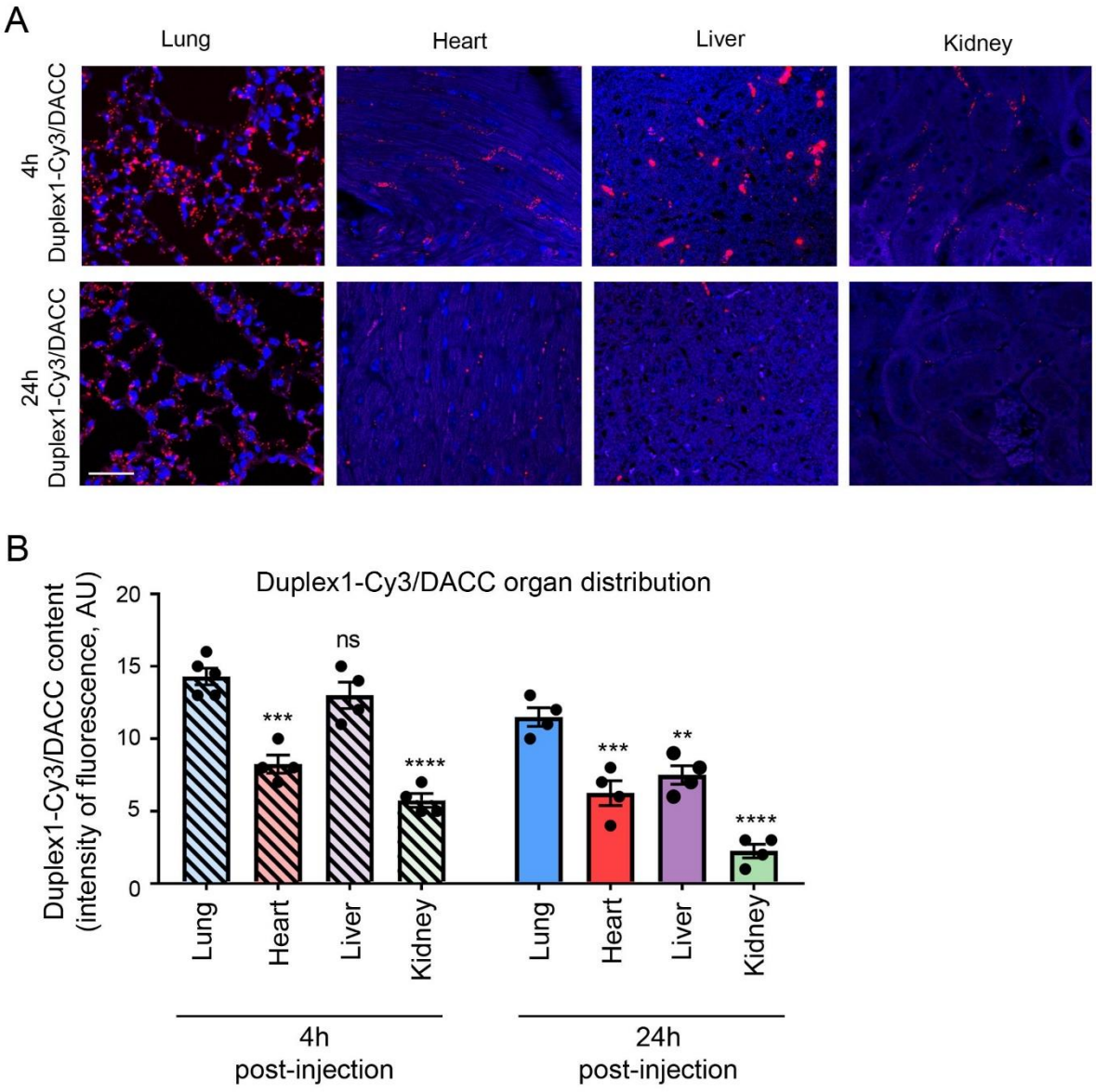

Figure S1. Distribution of fluorescent RNA marker delivered in DACC liposomes in mouse lung, heart, liver and kidney. siRNA-Cy3/DACC (Duplex1-Cy3/DACC) or (vehicle only) were delivered to mice by iv injection and tissue distribution of fluorescent siRNA was studied 4 hr or 24hr later. (A) Representative images and (B) a corresponding graph showing distribution of Duplex1-Cy3/DACC in different organs, as indicated. In (A) nuclei are blue (DAPI), while siRNACy3 is red. Bar=25 μm. In (B) **p<0.01, ***p<0.001, ****p<0.0001, comparisons with 24h lung (for 24h group) or 4h lung (for 4h group), as appropriate; N=4-5.

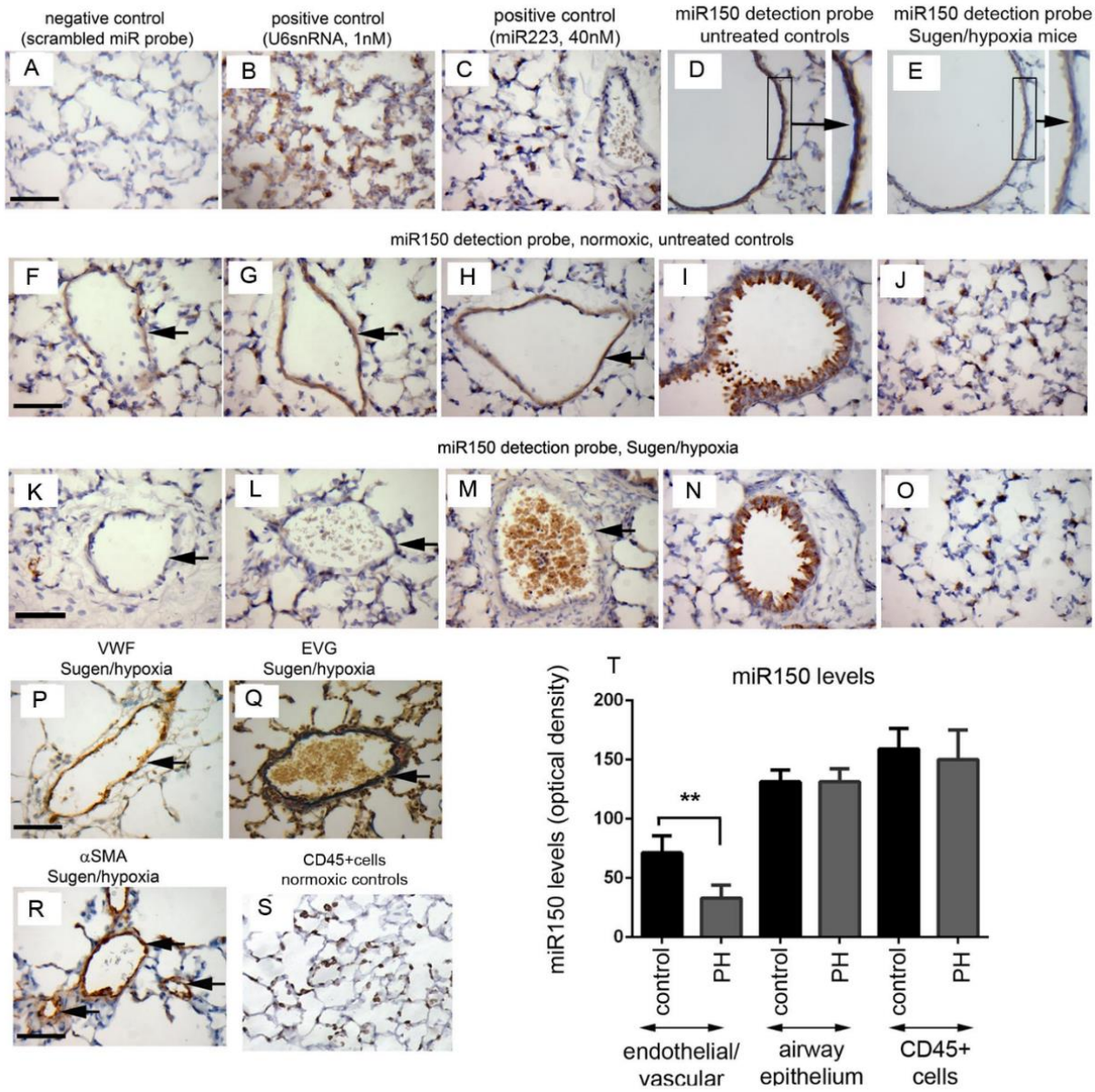

Figure S2. **miR-150 levels are decreased in the endothelium of pulmonary hypertensive hypoxia/Sugen mice; in situ hybridization.** (A-C) negative and positive controls; (D, E) miR-150 in pulmonary vascular endothelium in control mice and Sugen/hypoxia mice, as indicated; (F-H) miR-150 staining in the small intrapulmonary vessels (arrows) in control lungs; (I and J) corresponding miR-150 staining in the airway epithelium and leukocytes, respectively. (K-M) miR-150 staining in intrapulmonary vessels of Sugen/hypoxia mice; (N and O) corresponding miR-150 staining of the airway epithelium and leukocytes in Sugen/hypoxia lungs, respectively. (P, Q and R show vWF, EVG and αSMA staining of the remodelled intrapulmonary vessels in Sugen/hypoxia mice. (S) localization of leukocytes (CD45+cells) in control lung; Bar=40μm. The graph shows relative changes in miR-150 levels in endothelial/vascular tissues, airway epithelium and $CD45^+$ cells in lung tissues from control and PH mice (3 mice/group, 10 vessels/mouse). Optical density of selected 7-10 regions of interest within the endothelial layer or 10 $CD45^+$ cells was measured with Image Pro Plus software. Bars are means ± SEM. *$p<0.05$, comparison with control. n=5/group

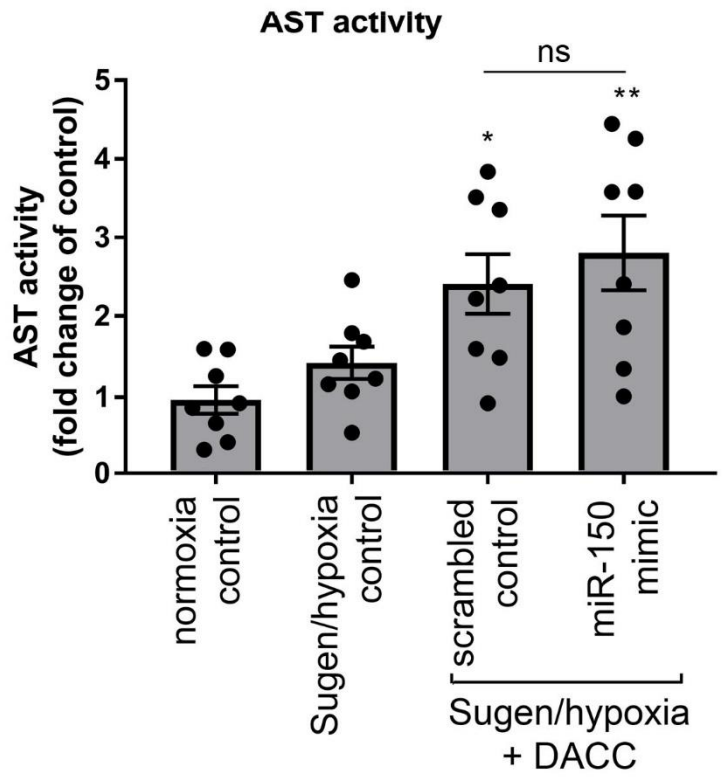

Figure S3. Liver aspartate aminotransferase (AST) activity in mice. AST activity (nmole glutamate/min/mL) was measured in liver tissues from untreated normoxic mice, untreated Sugen/hypoxia mice, Sugen/hypoxia mice treated with DACC/miRNA scrambled controls and Sugen/hypoxia mice treated with DACC/miR-150 mimic (N=8/group). AST activity is shown as fold-change of normoxic controls. Bars are means ± SEM. *$p<0.05$; **$p<0.01$, comparison with normoxic control; one-way ANOVA with Tukey post-test.

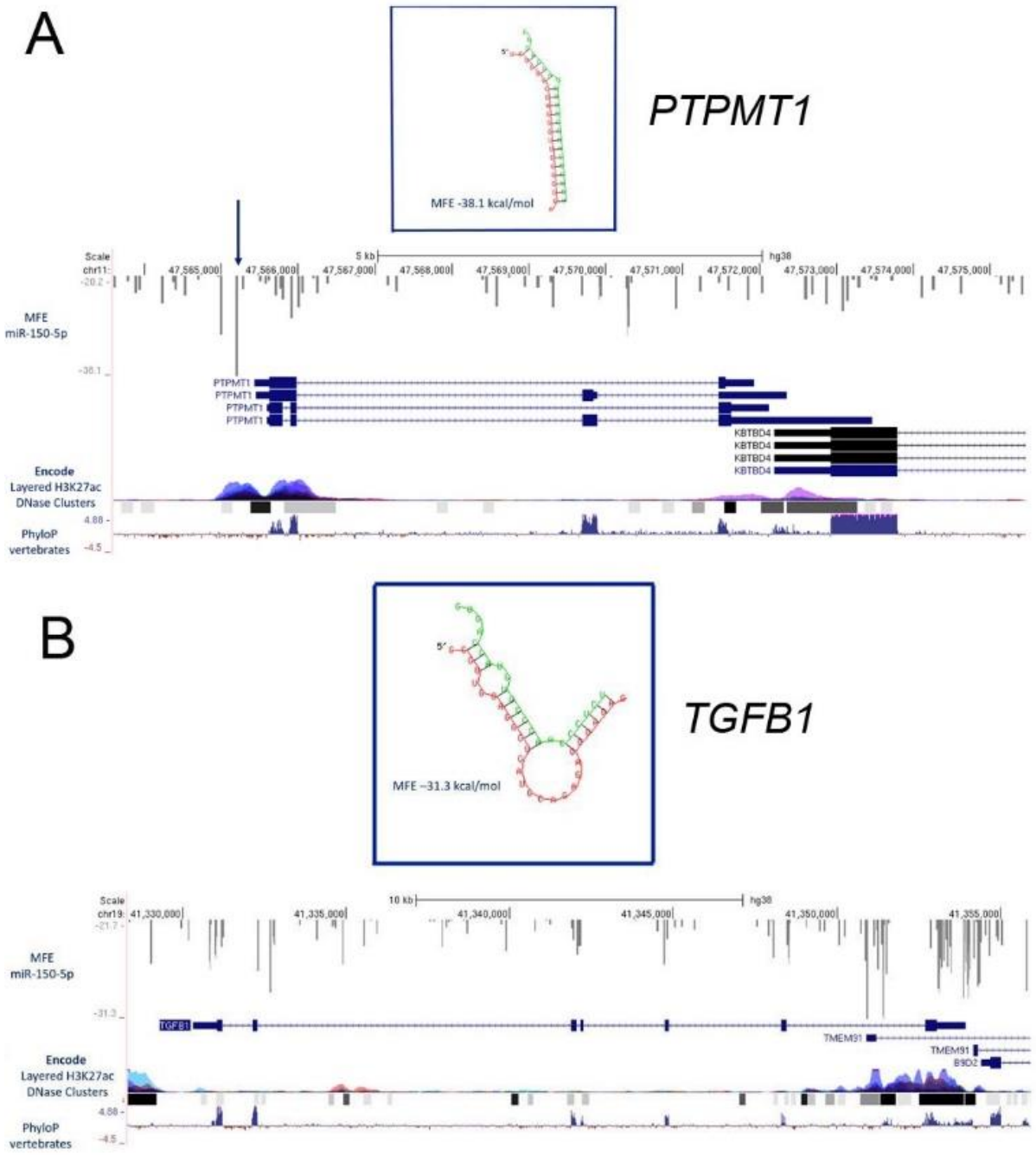

Figure S4. Predicted miR-150 binding sites.

(A) RNAhybrid identified 70 putative miR-150 (MIMAT0000451) predicted binding sites to *PTPMT1* (chr11:47563600-47575461) with minimum free energy (MFE) ranges between -20.2 kcal/mole and -38.1 kcal/mole. The top MFE event (-31.3 kcal/mole) occurred within the promoter region of *PTPMT1* (inset). (B) RNAhybrid gave in-silico predictions for 100 binding events of miR-150 to TGFB1 (chr19:41328324-41355922) with MFE ranges between -21.7 kcal/mole and -31.3 kcal/mole. The top MFE event (-31.3 kcal/mole) occurred within the first intron of TGFB1 (inset). Images are adapted from UCSC Genome Browser.

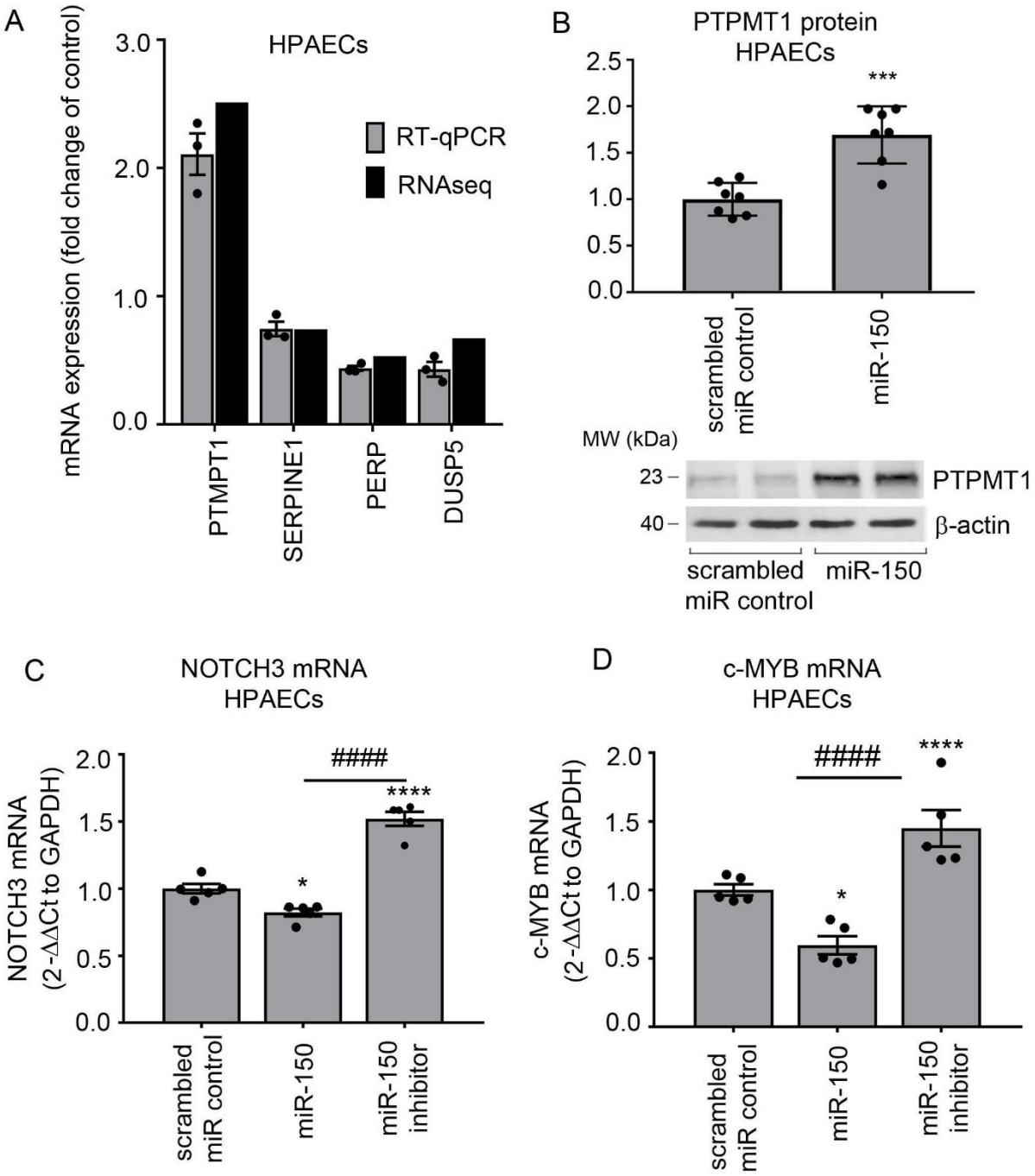

Figure S5. RNA-Sequencing validation. RNA-Sequencing results (black bars) were validated for selected miR-150-regulated genes by RT-qPCR. (A) PTPMT1, SERPINE1, PERP, DUSP5 mRNA levels expressed as fold change of transfection control. (B) Graph shows fold-change in PTPMT1 protein expression in HPAECs transfected with miR-150 mimic, compared with scrambled control. A corresponding representative western blot is shown below the graph. (C) NOTCH3 and (D) c-MYB in HPAECs transfected with scrambled miR, miR-150 mimic or inhibitor. Bars are mean fold-changes of control ± SEM. *p<0.05; ****p<0.0001, comparison with scrambled control; $^{\#\#\#\#}$p<0.0001, comparison, as indicated. In (A) N=3, in (B) N=7, in (C, D) N=5.

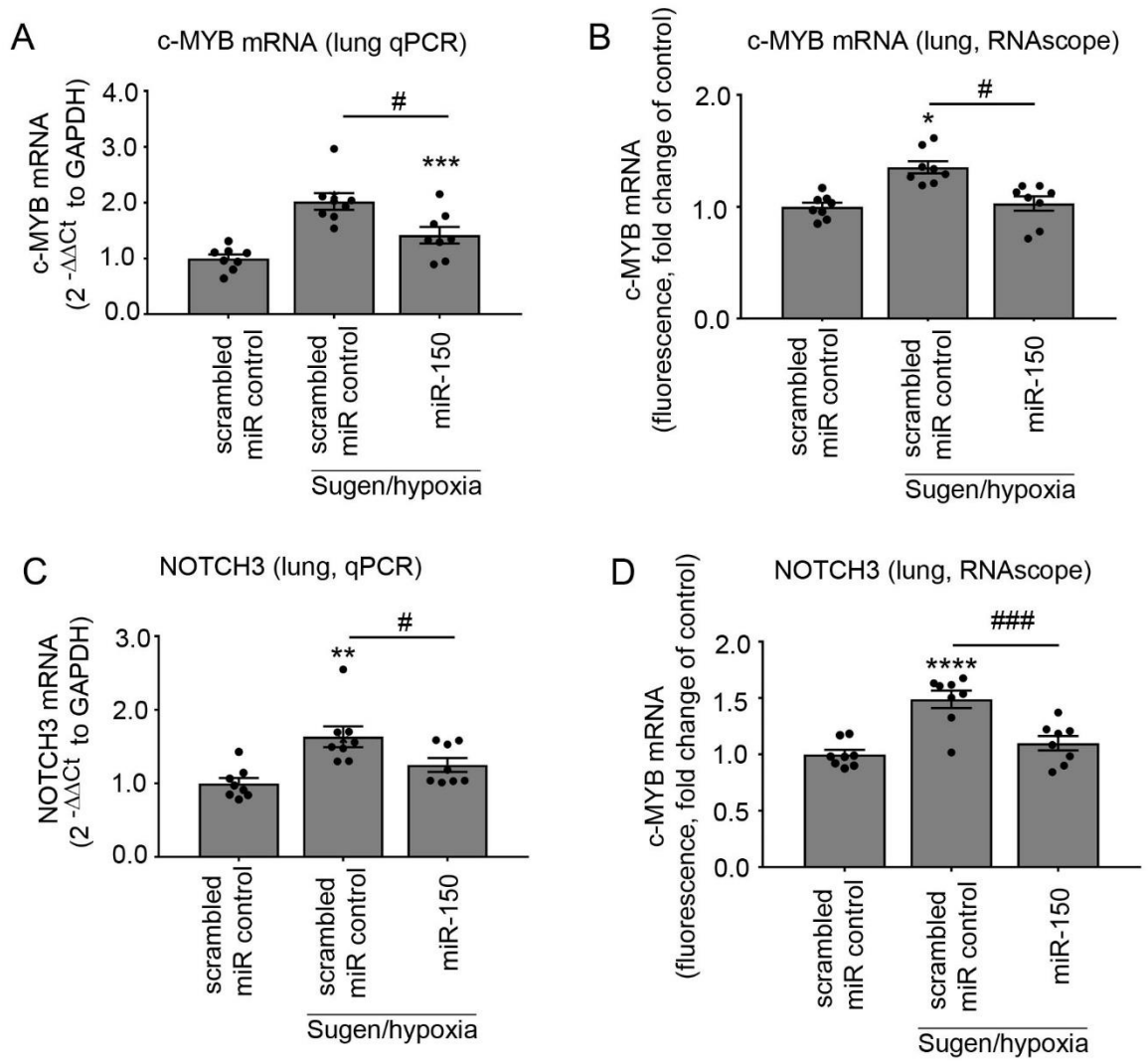

Figure S6. Expression levels of miR-150-regulated genes *in vivo*. (A, B) c-MYB and (C, D) NOTCH3 mRNA evaluated by qPCR or RNAscope in situ hybridization analysis in lungs of healthy controls and Sugen/hypoxia mice treated, as indicated. Bars are mean fold-changes of control ± SEM. *$p<0.05$; ****$p<0.0001$, comparison with scrambled control; $^{\#}p<0.05$, $^{\#\#\#}p<0.001$, comparisons, as indicated. N=8.

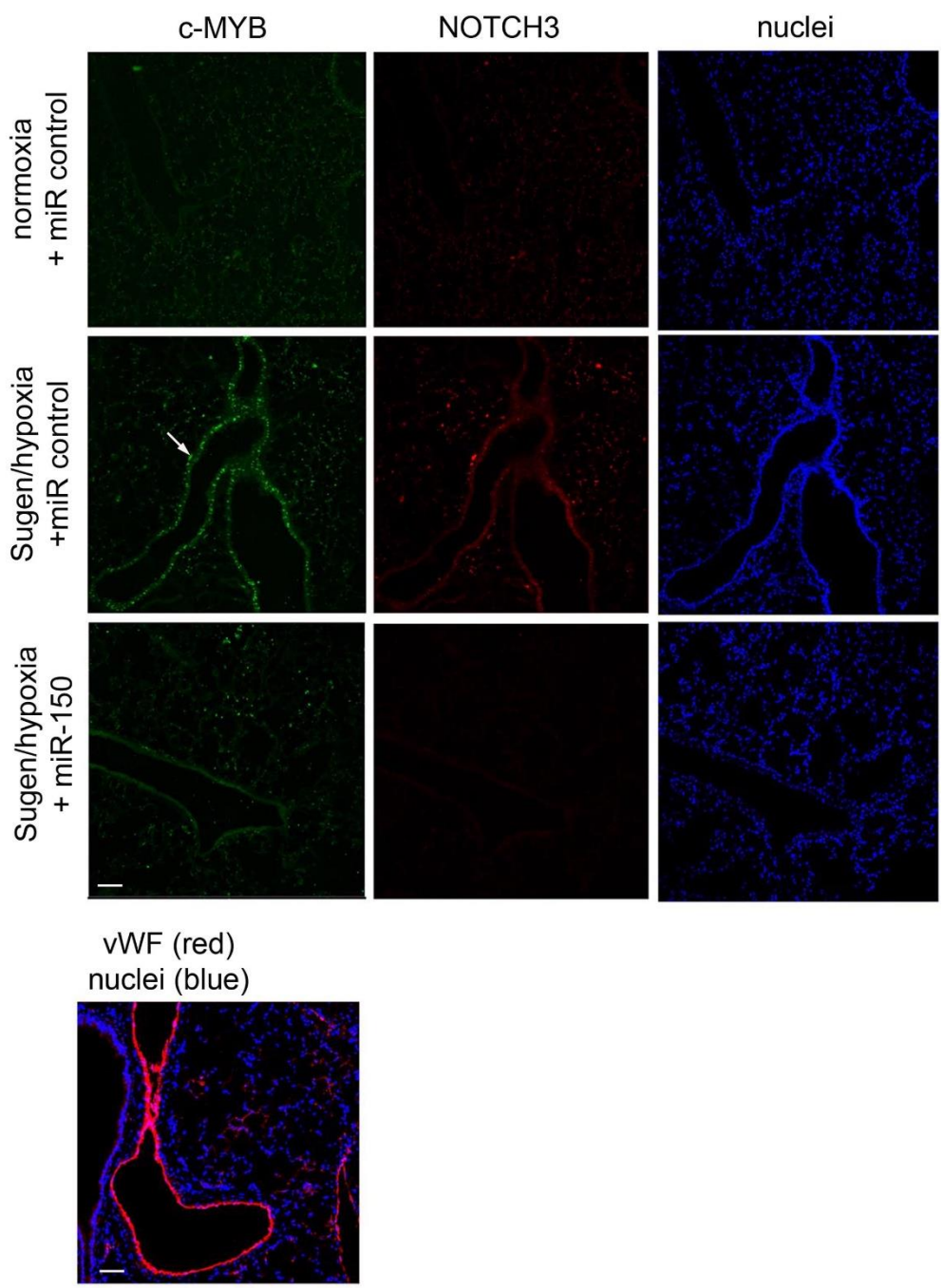

Figure S7. Representative images of c-MYB (green) and NOTCH3 (red) mRNA staining in mouse lungs. Transcripts were identified by the RNAscope fluorescent *in situ* hybridization in lungs from normoxic and Sugen/hypoxia control mice (treated with DACC/scrambled miRNA control) and Sugen/hypoxia mice treated with DACC/miR-150, as indicated. Nuclei are stained in blue (DAPI) N=6. Image bellow the main panel shows vWF staining (red) in healthy lung to visualise distribution of endothelial cells. Bar=50µm.

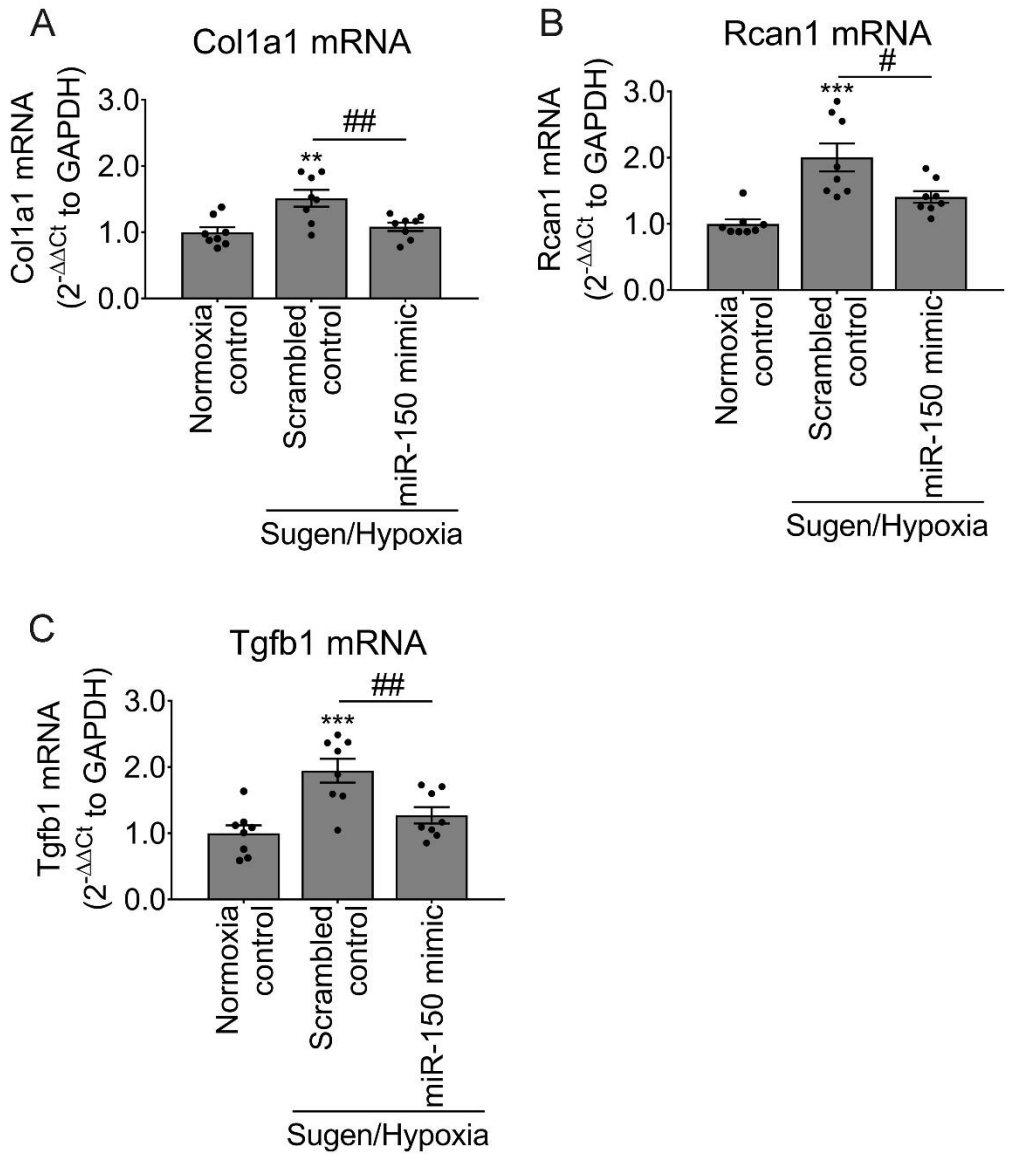

Figure S8. miR-150 supplementation reduces expression of pro-fibrotic genes in the right ventricle of Sugen/hypoxia mice. (A-C) show expression changes in Collagen 1 (Col1a1), regulator of calcineurin 1 (Rcan1) and TGFB1. In graphs, bars are mean fold-changes of control ± SEM; one-way ANOVA with Tukey post-test. ***$p<0.001$, comparison with normoxia control. $^{\#}p<0.05$, $^{\#\#}p<0.01$, comparisons with scrambled control. N=8

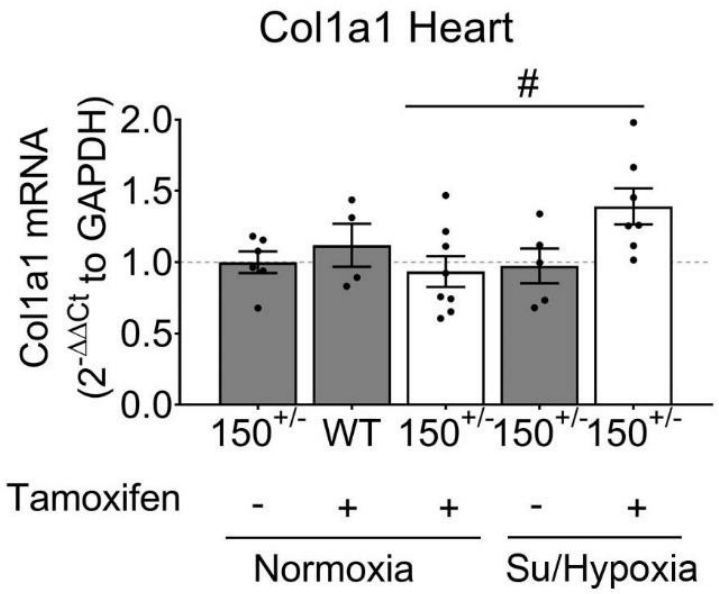

Figure S9. Endothelial deletion of miR-150 increases collagen 1 expression in the heart. Col1a1 mRNA levels in the right ventricle of wildtype and miR-150iEC-KO (miR-150$^{+/-}$) mice in normoxia or Sugen/hypoxia, with and without tamoxifen, as indicated. Empty bars mark miR-150-deficient animals. Bars show mean fold-changes of control ± SEM; one-way ANOVA with Tukey post-test. $^{\#}p<0.05$, comparisons, as indicated. N=5-8.

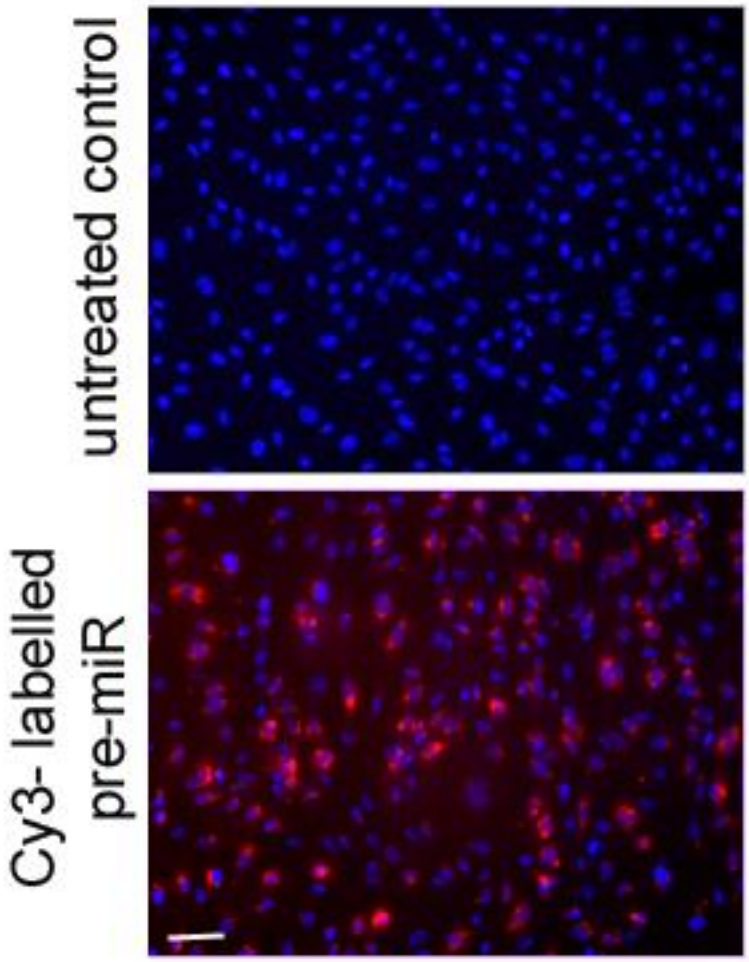

Figure S10. Transfection efficiency in HPAECs transfected with fluorescently-labelled Cy3-pre-miR mimic (20 nM; lower panel). Transfected cells are red, whereas nuclei are blue (DAPI). Bar=50 μm.

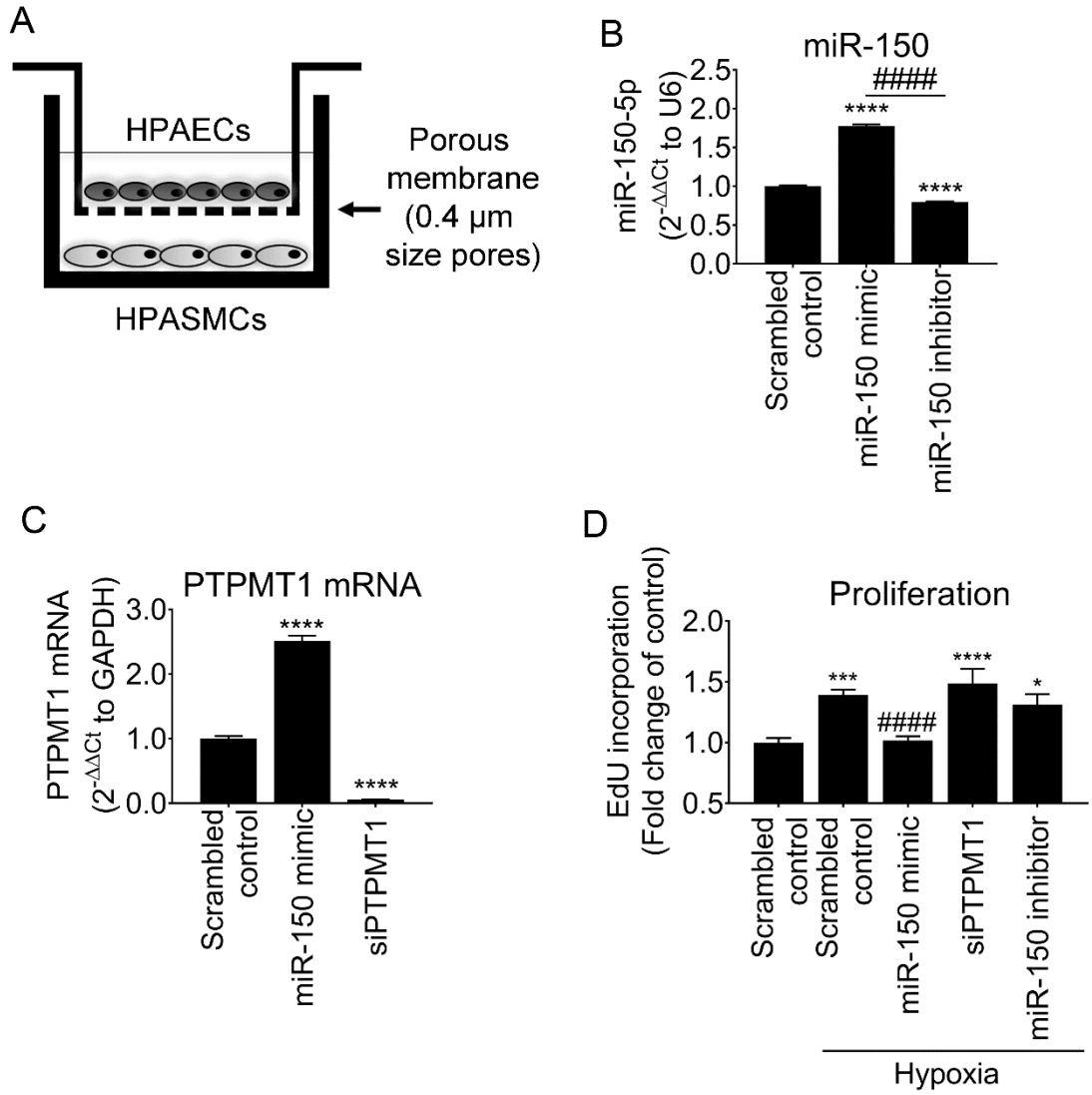

Figure S11. Effects of miR-150 transfection and PTPMT1 silencing on smooth muscle cell proliferation. (A) Schematic representation of non-contact co-culture of HPAECs and HPASMCs. Endothelial cells were seeded in the top chamber, whereas smooth muscle cells were seeded in the bottom of the plate. A porous (0.4 μm pore size) membrane separated the two cell types. (B) miR-150 expression levels in HPASMCs transfected with miR-150 mimic or inhibitor. (C) PTPMT1 expression levels in smooth muscle cells transfected with miR-150 mimic or siPTPMT1. (D) Proliferation of HPASMCs co-cultured with HPAECs transfected with miR-150 mimic, siPTPMT1 and miR-150 inhibitor for 48h. One-way ANOVA with Tukey post-test. Bars are means ± SEM. N =3 in (B and C) and N=5 in (D).

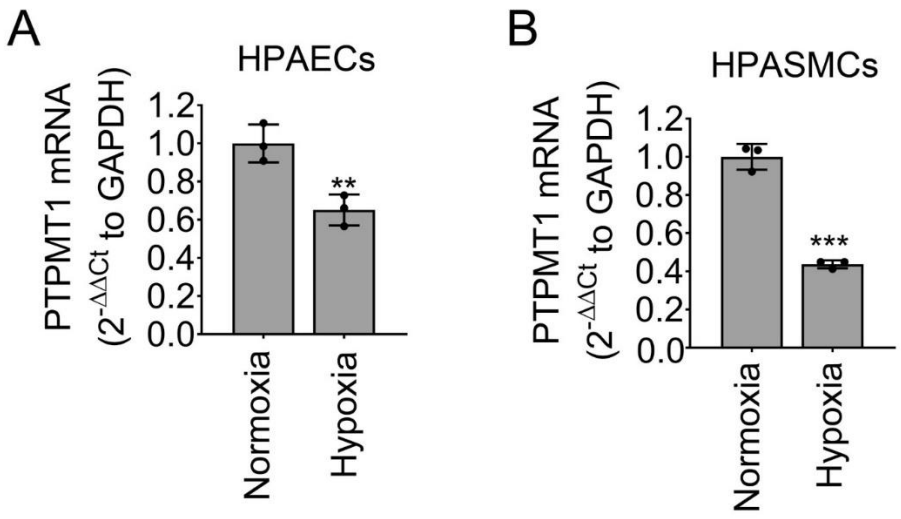

Figure S12. Effects of hypoxia on PTPMT1 expression in HPAECs and HPASMCs. PTPMT1 mRNA expression was measured in (A) HPAECs and (B) HPASMCs under normoxic or hypoxic (24 hours) conditions. In graphs, bars are mean fold-changes of control ± SEM; Student t-test. **p<0.01; ***p<0.001, comparison with normoxic controls, N=3.

Supplementary References

1. Fehring, V, Schaeper, U, Ahrens, K, Santel, A, Keil, O, Eisermann, M, *et al.* (2014). Delivery of therapeutic siRNA to the lung endothelium via novel Lipoplex formulation DACC. *Mol Ther* **22**: 811-820.
2. Wang, Y, Nakayama, M, Pitulescu, ME, Schmidt, TS, Bochenek, ML, Sakakibara, A, *et al.* (2010). Ephrin-B2 controls VEGF-induced angiogenesis and lymphangiogenesis. *Nature* **465**: 483-486.
3. Pitulescu, ME, Schmidt, I, Benedito, R, and Adams, RH (2010). Inducible gene targeting in the neonatal vasculature and analysis of retinal angiogenesis in mice. *Nat Protoc* **5**: 1518-1534.
4. Wojciak-Stothard, B, Abdul-Salam, VB, Lao, KH, Tsang, H, Irwin, DC, Lisk, C, *et al.* (2014). Aberrant chloride intracellular channel 4 expression contributes to endothelial dysfunction in pulmonary arterial hypertension. *Circulation* **129**: 1770-1780.
5. Wang, F, Flanagan, J, Su, N, Wang, LC, Bui, S, Nielson, A, *et al.* (2012). RNAscope: a novel in situ RNA analysis platform for formalin-fixed, paraffin-embedded tissues. *J Mol Diagn* **14**: 22-29.
6. Sindi, HA, Russomanno, G, Satta, S, Abdul-Salam, VB, Jo, KB, Qazi-Chaudhry, B, *et al.* (2020). Therapeutic potential of KLF2-induced exosomal microRNAs in pulmonary hypertension. *Nat Commun* **11**: 1185.
7. Love, MI, Huber, W, and Anders, S (2014). Moderated estimation of fold change and dispersion for RNA-seq data with DESeq2. *Genome Biol* **15**: 550.

8. Patro, R, Duggal, G, Love, MI, Irizarry, RA, and Kingsford, C (2017). Salmon provides fast and bias-aware quantification of transcript expression. *Nat Methods* **14**: 417-419.
9. Anders, S, Pyl, PT, and Huber, W (2015). HTSeq--a Python framework to work with high-throughput sequencing data. *Bioinformatics* **31**: 166-169.
10. Hochberg, Y, and Benjamini, Y (1990). More powerful procedures for multiple significance testing. *Stat Med* **9**: 811-818.
11. Farrand, L, Kim, JY, Im-Aram, A, Suh, JY, Lee, HJ, and Tsang, BK (2013). An improved quantitative approach for the assessment of mitochondrial fragmentation in chemoresistant ovarian cancer cells. *PLoS One* **8**: e74008.
12. Martinez, K, and Cupitt, J (2005). VIPS - a highly tuned image processing software architecture. *Ieee Image Proc*: 2485-2488.
13. Hong, Z, Kutty, S, Toth, PT, Marsboom, G, Hammel, JM, Chamberlain, C, *et al.* (2013). Role of dynamin-related protein 1 (Drp1)-mediated mitochondrial fission in oxygen sensing and constriction of the ductus arteriosus. *Circ Res* **112**: 802-815.